Design, synthesis and biological evaluation of novel SARS-CoV-2 3CL^{pro} covalent inhibitors.

Julia Stille,[#,1] Jevgenijs Tjutrins,[#,1] Guanyu Wang,[#,1] Felipe A. Venegas,[#,1] Christopher Hennecker,[1] Andres Mauricio Rueda [1] Itai Sharon,[2] Caitlin E. Miron,[1] Sharon Pinus,[1] Anne Labarre,[1] Jessica Plescia,[1] Mihai Burai Patrascu,[1] Xiaocong Zhang,[1] Alexander S. Wahba,[1] Danielle Vlaho,[1] Mitchell J. Huot,[1] T. Martin Schmeing,[2] Anthony K. Mittermaier,[1] and Nicolas Moitessier*,[1]*

[1] Department of Chemistry, McGill University, 801 Sherbrooke St W, Montreal, QC, Canada H3A 0B8. [2] Department of Biochemistry, McGill University, 3649 Promenade Sir William Osler Montreal, QC, Canada H3G 0B1

*corresponding authors: nicolas.moitessier@mcgill.ca; anthony.mittermaier@mcgill.ca

[#] These authors contributed equally to this work.

Abstract

Severe diseases such as the ongoing COVID-19 pandemic, as well as the previous SARS and MERS outbreaks, are the result of coronavirus infections and have demonstrated the urgent need for antiviral drugs to combat these deadly viruses. Due to its essential role in viral replication and function, 3CL^{pro} has been identified as a promising target for the development of antiviral drugs. Previously reported SARS-CoV 3CL^{pro} non-covalent inhibitors were used as a starting point for the development of covalent inhibitors of SARS-CoV-2 3CL^{pro}. We report herein our efforts in design and synthesis which led to submicromolar covalent inhibitors when the enzymatic activity of the viral protease was used as a screening platform.

Introduction

Coronaviruses. Coronaviruses (CoV) are a large family of viruses associated with the common cold, as well as far more serious diseases including Severe Acute Respiratory Syndrome (SARS, caused by SARS-CoV infection), which made headlines worldwide in 2002-2003 with over 700 deaths including 43 in Canada,[1] and the Middle East Respiratory Syndrome (MERS, caused by MERS-CoV infection), which was reported in Saudi Arabia in 2012 and killed over 900.[2] The current 2019-2020 outbreak of novel coronavirus (COVID-19, caused by SARS-CoV-2 infection) and the discovery of animal reservoirs provide significant motivation for the development of potent therapeutics against these viruses to prevent future outbreaks.[3,4]

SARS, MERS, and COVID-19 are respiratory illnesses characterized by fever, cough, and shortness of breath, posing significant danger to patients. The fatality rates for those infected with SARS-CoV and MERS-CoV are estimated at about 10% and 35%, respectively.[1,2] Early estimates for SARS-CoV-2 are on the order of 0.5 to 4%, although this number could change substantially as more accurate information on the numbers of infections and deaths becomes available.[5] In contrast to SARS and MERS, COVID-19 has rapidly spread worldwide despite the severe restrictions imposed in many countries, and the number of deaths now exceeds 2.7 million.[6]

Vaccines and therapeutics. While vaccines are a central pillar of our efforts to end our current deadly phase of the COVID-19 pandemic, therapeutics offer a complementary approach with many distinct advantages. For example, oral therapeutics tend to be easy to store and administer and need only be given to the small minority of patients suffering more serious symptoms. In contrast, a large proportion of the population must be inoculated for vaccines to be effective and mRNA-based vaccines require complex logistics to maintain the cold chain, leading to enormous challenges in production, supply and administration. In addition, large vaccine campaigns require public compliance and amplifies the number of people suffering from adverse reactions to medication. Importantly, vaccines primarily induce an immune response against the spike protein,[7] while current and future variants of concern have mutations in this protein that could allow them to evade immunity. In contrast, antiviral therapeutics can target a wide range of proteins including viral proteases (3CL^{pro}, PL^{pro}), the RNA-dependent RNA polymerase (RdRp) and RNA helicase. Therefore, they can be equally effective against strains of the virus with mutations that escape spike-based vaccination or herd immunity. Finally, some groups (pregnant and

breastfeeding women, people with allergies, young children or people with other conditions) may be at risk and alternative treatments (e.g., oral therapeutics) must be available.

Coronavirus (CoV) and 3-Chymotrypsin-like Protease Inhibition. Coronaviruses express 3-chymotrypsin-like cysteine proteases (3CL^{pro}), also referred to as the main proteases (Mpro) or nsp5 (non-structural protein 5), which feature a Cys-His catalytic dyad (Cys^{145}, His^{163}) and is required for viral replication and infection. 3CL^{pro} enzymes were identified early on as attractive targets for antiviral development, resulting in several inhibitors and structures of SARS-3CL^{pro}-inhibitor complexes (eg, PDB codes: 4TWY, 2ZU5, 2ALV.[8]) The 3CL^{pro} enzymes from SARS-CoV and SARS-CoV-2 share nearly 80% identity,[9,10] suggesting that many of the lessons learned for developing SARS therapeutics can be applied to COVID-19. As a note, 3CL^{pro} is not limited to coronaviruses but is also a drug target for the development of antivirals against noroviruses (such as the one involved in gastroenteritis[11]) or antivirals against enteroviruses (e.g., antiviral drug 3CLpro-1[12] targeting the hand, foot, and mouth disease enterovirus 71 and **Rupintrivir** originally developed to fight rhoniviruses[13]).

Covalent Inhibitors. The quest for novel antivirals against SARS-CoV and, more recently, SARS-CoV-2 has been intense, and several viral enzyme inhibitors and crystal structures of enzyme-inhibitor complexes have been reported (eg, PDB codes: 6M2N, 6XQU, 6WQF).[14] The presence of a catalytic cysteine residue in the active site makes 3CL^{pro} amenable to covalent inhibition, a strategy that was successfully employed following the SARS-CoV pandemic (SARS). In fact, many of the reported SARS-CoV inhibitors feature a reactive group, such as an α-ketoamide, epoxide, aziridine, α,β-unsaturated ester (Michael acceptor), or α-fluoroketone, which forms a covalent bond with the catalytic cysteine residue (Cys^{145}), as confirmed by X-ray crystallography (e.g., PDB code: 5N19).[14] Fortunately, a crystal structure of the SARS-CoV-2 3CL^{pro} with a covalent peptidic inhibitor bound to cysteine residue (Cys^{145}), was quickly elucidated (PDB code: 6LU7), followed by many others.[15] This pseudo-peptidic inhibitor, an analogue of **Rupintrivir** (tested on SARS[16] and COVID-19[17]), has been the starting point for a number of drug discovery campaigns.[18-22] Recently, a 3CL^{pro} inhibitor (**PF-0730814**, Figure 1) entered Phase 1 clinical trials[20] and smaller, more drug-like inhibitors such as 2 have been devised (ref).[23,24] More recently, efforts to convert Perampanel, a known antiepileptic drug that is also a weak 3CL^{pro} inhibitor by Jorgensen and co-workers used a combination of computational and experimental investigation to identify **3**, a potent SARS-CoV-2 3CL^{pro} inhibitor (Figure 1).[25]

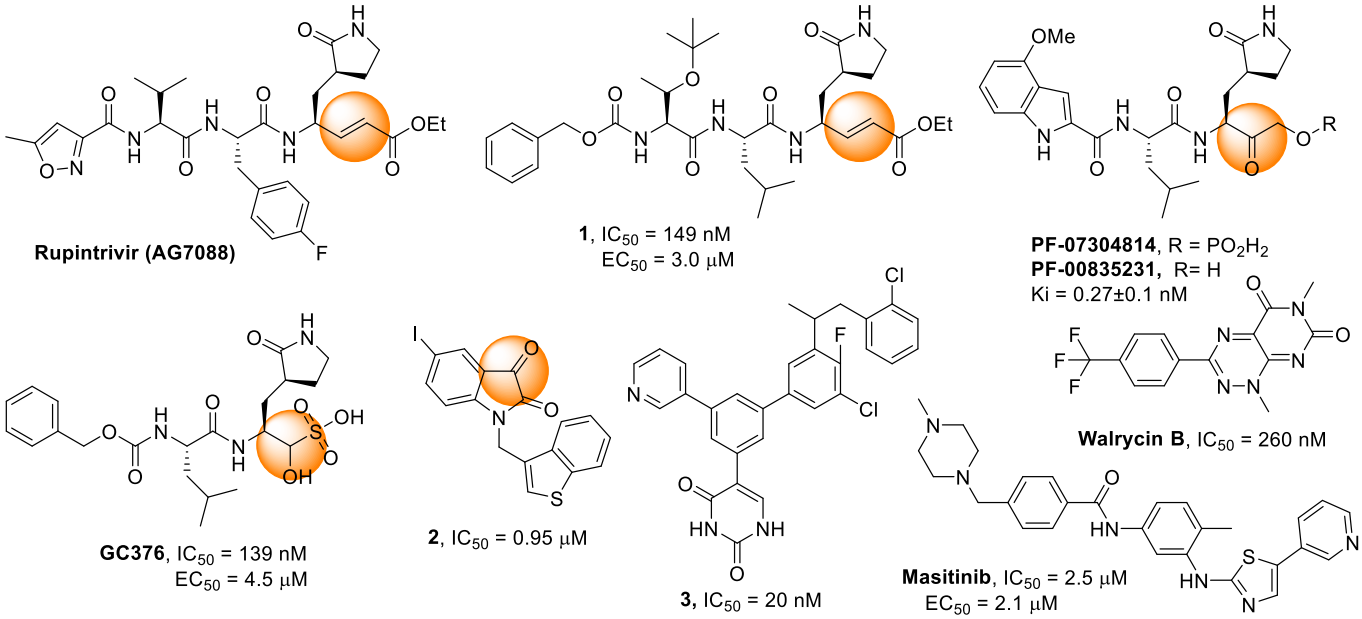

Figure 1. Reported covalent SARS-CoV-2 3CL^{pro} inhibitors **1, GC376**[19] and **PF-0730814**,[26] reported non-covalent inhibitors **Masitinib**[27] and **Walcyrin B**.[28] Reported inhibitors of SARS-CoV 3CL^{pro} **2**[23] and **3**.[25] Orange spheres indicate the warheads for covalent binding.

As described in our recent review,[29] covalent drugs can be extremely effective and useful pharmaceuticals, yet they have been largely ignored in most drug design endeavours and particularly in those concerning structure-based drug design. Concerns about their potential off-target reactivity and toxicity have often been raised.[30] Despite these concerns, there are many examples of covalent drugs on the market, including two of the ten most widely prescribed medications in the U.S., as well as several other common drugs like aspirin and penicillin.[29] The advantages of covalent drugs are becoming increasingly recognized: they have extremely high potencies, long residence times, and high levels of specificity.[31] Although skepticism persists, many pharmaceutical companies are embracing covalent drugs as exemplified by **Neratinib** (Nerlynx®, Pfizer) and **Afatinib** (Gilotrif®, Boehringer-Ingelheim).

3CL^{pro} inhibitor design. Many of the structure-based studies related to COVID-19 to date have employed virtual screening and machine learning techniques. Several ***potential*** 3CL^{pro} inhibitors have been identified, however experimental verification has lagged.[32-34] As of today, much of the research has focused on peptidic substrate-like inhibitors (Figure 1). There is currently a need for the development of drug-like inhibitors with synthetically accessible scaffolds that will allow for more thorough investigations of structure-activity relationships. We thought to benefit from our team's expertise in covalent inhibition and from our software that enables automated docking and virtual screening of covalent inhibitors, which

is not possible with most commercial packages. We present herein our efforts towards the development of novel potent covalent inhibitors of 3CL^{pro}.

Chemistry

Inhibitor design through covalent docking. In the past years, we have successfully applied covalent docking to the design and discovery of prolyl oligopeptidase inhibitors[35,36] and thought to apply a similar strategy to develop SARS-CoV-2 3CL^{pro} inhibitors. An investigation of the crystal structure of a non-covalent inhibitor (**X77**, Figure 2) bound to 3CL^{pro} of SARS-CoV-2 (PDB code: 6W63) suggested that it might be possible to modify this inhibitor by incorporating a covalent warhead in proximity to the catalytic cysteine residue. As shown in Figure 2, the sulphur atom of Cys^{145} is positioned at 3.2Å from the imidazole moiety. Thus, replacement of the imidazole with a covalent warhead appeared to be a promising strategy to improve the inhibitory potency of this non-covalent inhibitor. Additionally, this scaffold could be prepared via a 4-component Ugi reaction,[37] enabling a combinatorial approach that would provide an efficient synthetic method for preparing diverse analogues. This would provide a significant advantage in exploring structure-activity relationships when compared to previously reported inhibitors, as a wide range of covalent warheads could be readily incorporated into the same inhibitor scaffold. As a note, a consortium of research groups including a group at the Weizmann Institute of Science in Rehovot (Israel) took a very similar strategy although focusing primarily on non-covalent inhibitors.[15]

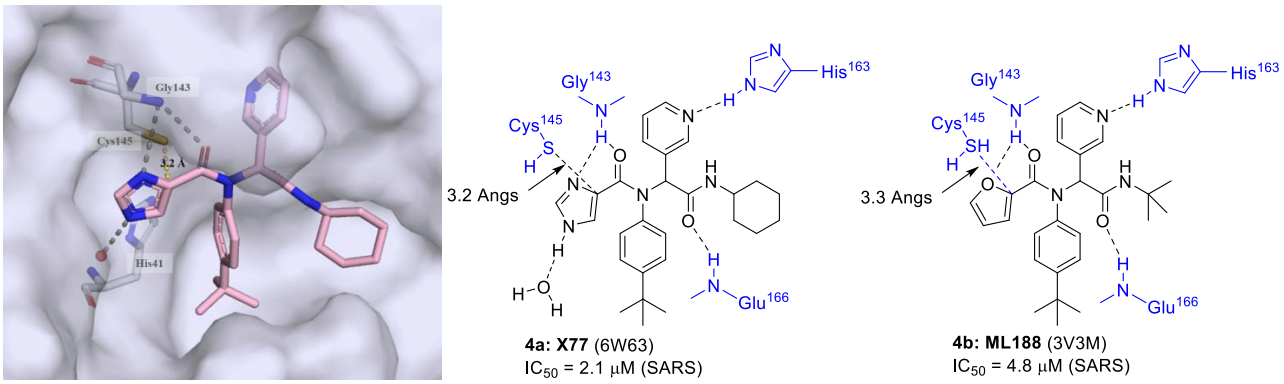

Figure 2. Imidazole of **4a** (**X77**) inhibitor and **4b** (**ML188**) interacting with HOH-518 (PDB codes: 6W63 and 3V3M).

To validate the design strategy, a virtual library of modified inhibitors was prepared based on incorporation of covalent warheads that could be accessed via a traditional or modified Ugi 4 component coupling (4CC) reaction. These compounds were docked to 3CL^{pro} (PDB code: 6W63) using our docking program, FITTED[38] (Figures 3 and 4). The docked poses (Figure 4) suggested that many of these modified

inhibitors would be able to maintain the same non-covalent interactions as the original non-covalent inhibitor while also positioning the warhead close enough to Cys^{145} to facilitate the formation of a covalent bond. While β-lactams and nitriles are well-established covalent warheads, their synthesis via modified Ugi reactions would result in analogues without the *tert*-butyl phenyl group. The formation of a covalent bond may not be enough to overcome the loss of this non-covalent interaction, as is suggested by a decreased docking score. Based on the promising docking results with multiple warheads, a small library of analogues was synthesized for experimental testing.

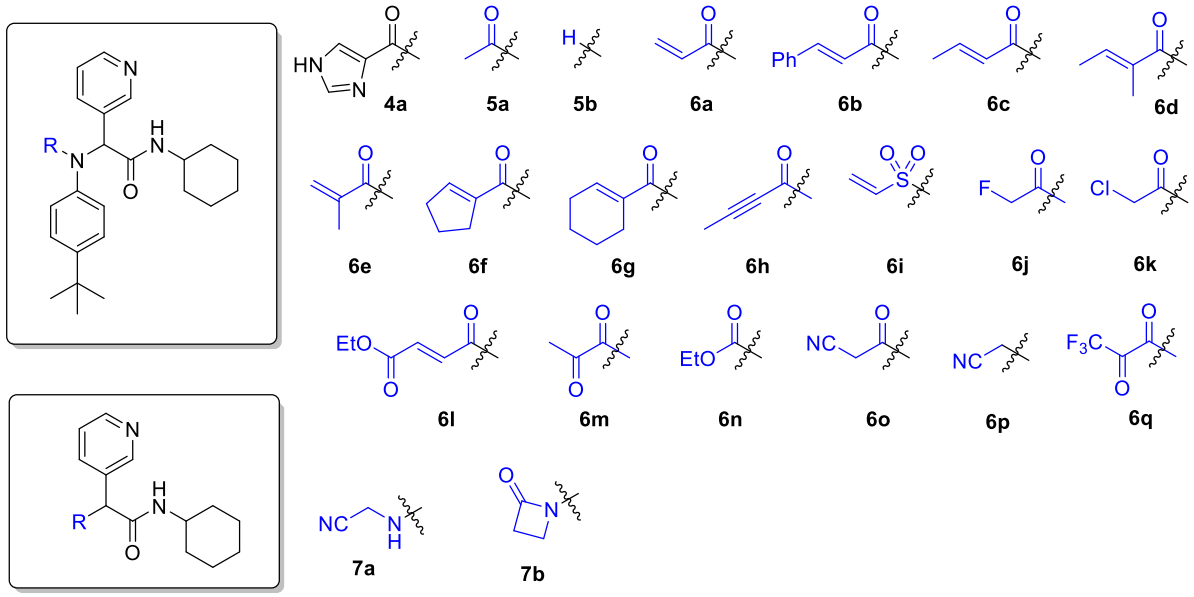

Figure 3. Selected covalent 3CL^{pro} inhibitors for synthesis. Compound **4a** (**X77**) is the original non-covalent lead compound.

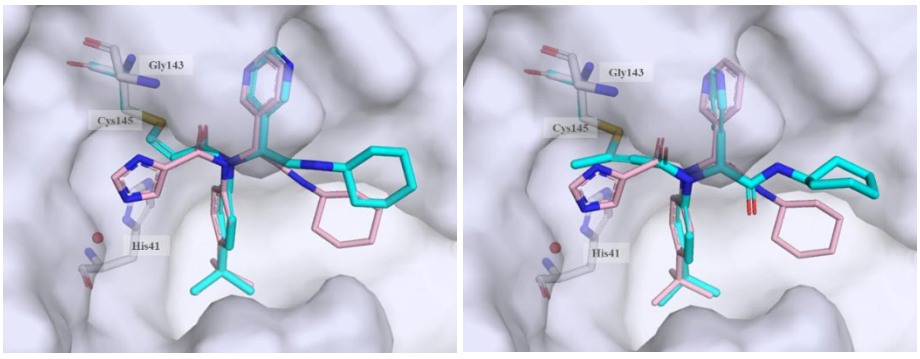

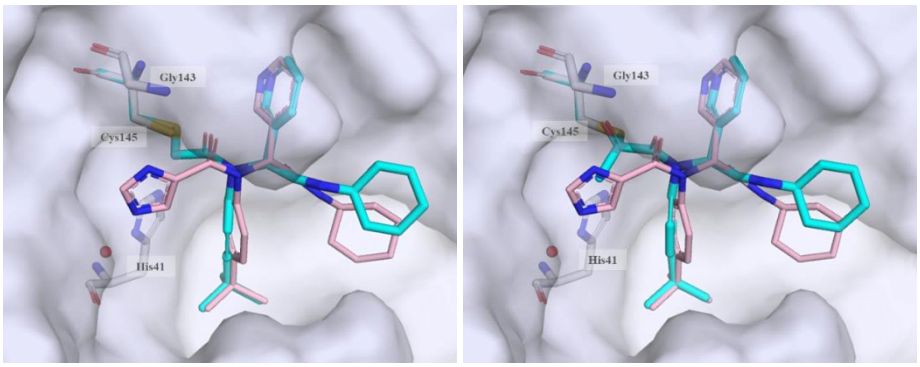

Figure 4. Selected docked binding modes of design covalent inhibitors (cyan) overlaid with the non-covalent inhibitor (co-crystallized) **4a** (light pink). Top left: **6a**, top right: **6h**, bottom left: **6k** and bottom right: **6m**.

Synthesis. Following a protocol reported by Jacobs *et al*,[37] a 4-component Ugi reaction was used to prepare analogues bearing 4 different classes of covalent warheads (alkene Michael acceptor, α-halo ketone, alkyne Michael acceptor, and α-ketoamide, Scheme 1).

Scheme 1[a]

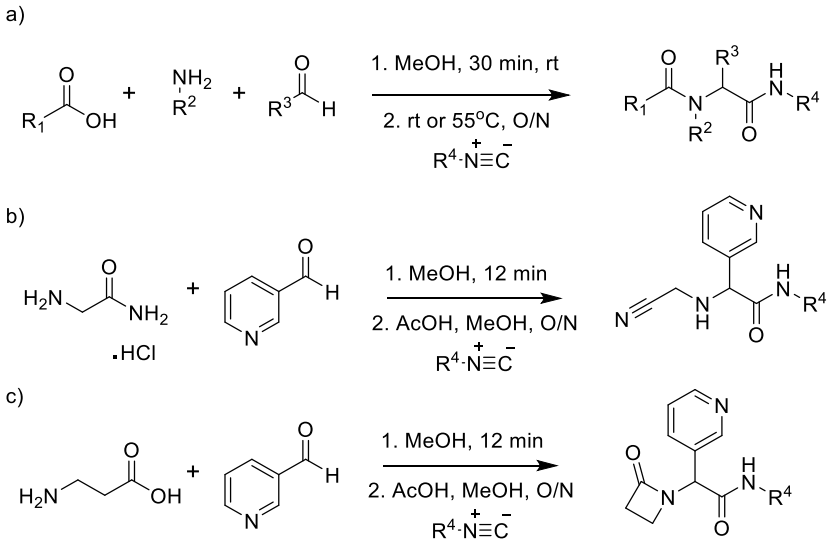

[a] a) carboxylic acid (1.0 mmol, 1.0 eq.), 4-*tert*-butylaniline (1.0 mmol, 1.0 eq.), 3-pyridinecarboxaldehyde (1.0 mmol, 1.0 eq.), cyclohexyl isocyanide (0.9 mmol, 0.9 eq.), MeOH (5 mL, 0.2 M), r.t., overnight. b) 3-pyridinecarboxaldehyde (2.0 mmol, 2.0 eq.), glycinamide hydrochloride (2.0 mmol, 2.0 eq.), triethylamine (2.0 mmol, 2.0 eq.), acetic acid (2.0 mmol, 2.0 eq.), cyclohexyl isocyanide (2.0 mmol, 2.0 eq.), MeOH (5 mL, 0.2 M), r.t., overnight, 79% yield. c) 3-pyridinecarboxaldehyde (1.0 mmol, 1.0 eq.), b-alanine (1.0 mmol, 1.0 eq.), cyclohexyl isocyanide (1.0 mmol, 1.0 eq.), MeOH (5 mL, 0.2 M), r.t., overnight, 54%.

A 3-component Ugi reaction was used to prepare the two additional analogues bearing a nitrile[39] and β-lactam[40] covalent warheads following reported procedures (Scheme 1b). This synthetic strategy was also employed to probe some of the features of this class of inhibitors. Thus the 3-pyrimidyl group was replaced by other heterocycles, the cyclohexyl was replaced by a *tert*-butyl group and the *tert*-butylphenyl was simplified into a toluyl.

In order to complete the synthesis of the analogues featuring various warheads not accessible through the Ugi 4CC, an intermediate was prepared and used to incorporate a vinylsulfonamide and a methyl carbamate (Scheme 2). In the meantime, this intermediate could be used to probe the presence of a group at this position.

Scheme 2[a]

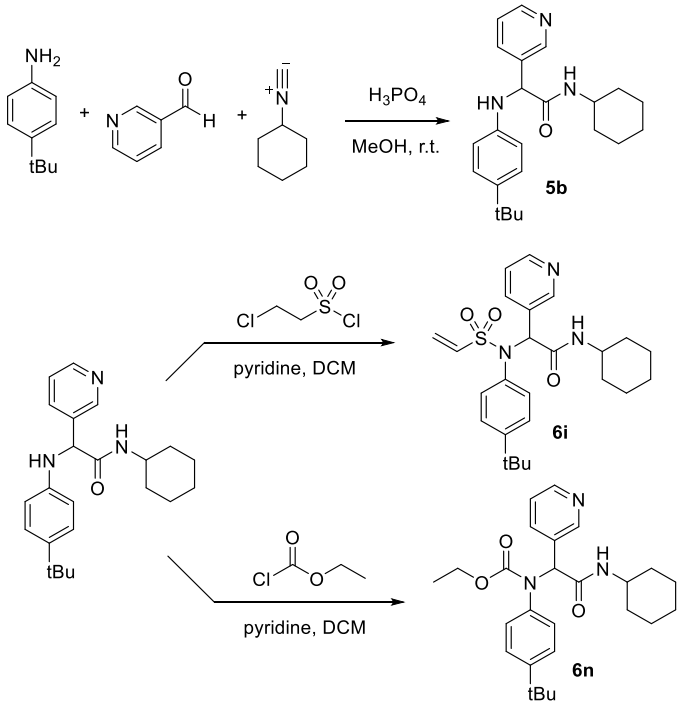

Results and Discussions

3CL^{pro} inhibition – covalent warheads. Our first focus was on the choice of the best covalent warhead. 17 potential warheads (compounds **6a-o** and **7a,b**) and four non-covalent analogues (**4a,b** and **5a,b**) were selected for synthesis. These compounds were next evaluated for their inhibitory potency using a fluorescence inhibition assay. An initial screening of these various synthesized compounds at 50 μM

resulted in ten compounds bearing covalent warheads presenting greater than 50% inhibition of 3CL^{pro} activity (Table 1). The most potent compounds (greater than 80% inhibition) were further evaluated (the fluorescence assay progress curves are shown in Figure S2). The recorded IC_{50} values are effective IC_{50}'s at 30-minute incubation time. Kinetics will then be measured on the identified most promising inhibitors (see below).

Table 1. Inhibitory potency against SARS-CoV-2 3CL^{pro}. Evaluation of warheads (R^1).

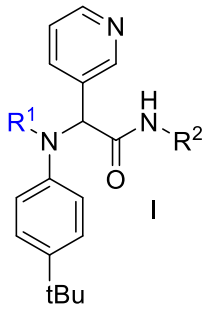

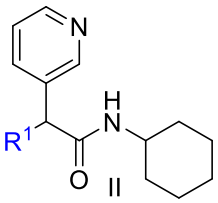

Entry	Scaffold	Cmpd	R^1	R^2	Inhibition (%)[a]	IC_{50} (μM) (K_i)
1	I	**4a (X77)**	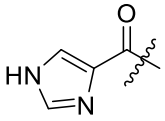	cHex	>95	4.1 ± 1.2
2	I	**4b (ML188)**	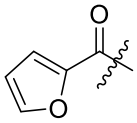	tBu	> 95	1.4 ± 0.4
3	I	**5a**		cHex	25 ± 8	nd[b]
4	I	**5b**		cHex	28 ± 3	nd[b]
5	I	**6a**	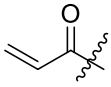	cHex	84 ± 1	11.1 ± 1.5
6	I	**6b**	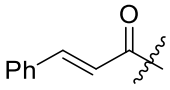	cHex	44 ± 6	nd[b]
7	I	**6c**	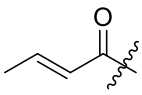	cHex	63 ± 5	nd[b]

8	I	**6d**	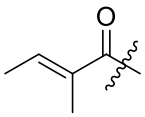	cHex	47 ± 2	nd[b]
9	I	**6e**	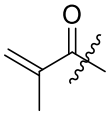	cHex	30 ± 1	nd[b]
10	I	**6f**	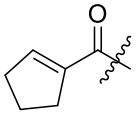	cHex	55 ± 10	nd[b]
11	I	**6g**	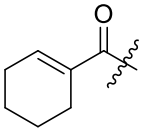	cHex	52 ± 1	nd[b]
12	I	**6h**	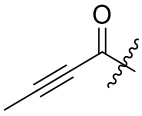	cHex	> 95	5.3 ± 0.8
13	I	**6i**	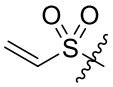	cHex	> 95	0.42 ± 0.11 (0.15 ± 0.04)
14	I	**6j**	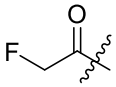	cHex	30 ± 7	nd[b]
15	I	**6k**	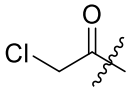	cHex	> 95	0.41 ± 0.13 (0.11 ± 0.04)
16	I	**6l**	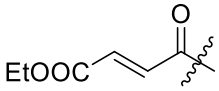	cHex	59 ± 6	nd[b]
17	I	**6m**	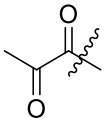	cHex	92 ± 1	5.2 ± 1.2
18	I	**6n**	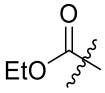	cHex	35.4 ± 3	nd[b]
19	I	**6o**	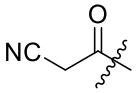	cHex	74.1 ± 1	6.95 ± 0.15
20	I	**6p**	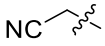	cHex	< 5	nd[b]

21	I	**6q**	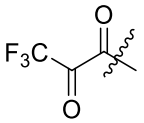	cHex	77 ± 4	nd[b]
22	II	**7a**	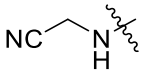	cHex	25 ± 1	nd[b]
23	II	**7b**	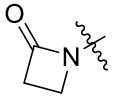	cHex	< 5	nd[b]

[a] The enzyme activity was measured with 150 nM 3CL^{pro} (114 nM after inhibitor addition) and 50 μM of each potential inhibitor with incubation time of 30 min. [b] not determined.

IC_{50} values (obtained at 11.7 μM substrate concentration) for the most promising inhibitors were evaluated and results are reported in Table 1. First, we observed that **4a** and **4b**, previously reported as low micromolar SARS-CoV 3CL^{pro} inhibitors (IC_{50} = 3.4 μM[41] and IC_{50} = 4.8 μM[37] respectively), also inhibit SARS-CoV-2 3CL^{pro} with similar potencies (Table 1, entries 1 and 2). Gratifyingly, some of the designed inhibitors, in particular **6a**, **6h, 6m, 6i, 6k** and **6o** also inhibited SARS-CoV-2 3CL^{pro}, some even with potency higher than the original non-covalent inhibitor with this incubation time. A closer look at the structures revealed that the most reactive and least hindered warheads (acrylamide, vinylsulfonamide, alkynylamide, α-chloro ketone and ketoamide) showed the highest activity. Interestingly, our two most potent inhibitors **6k** and **6i** (IC_{50} = 0.4 and 0.5 μM) were an order of magnitude more potent than the original non-covalent hit molecule (**4a**: IC_{50} = 4.1 μM).

Another observation is the significant loss of potency when removing the imidazole ring (compounds **4a** vs. **5a**). As illustrated in Figure 2, the basic imidazole nitrogen of the original inhibitor **4a** interacts with the Gly[143] backbone amide, an interaction also observed with the furan ring of **4b** (PDB code: 3V3M) or other heterocycles of the same chemical series.[37,42] This Gly amide together with Ser[144] and Cys[145] backbone amides form the oxyanion hole that contributes to the catalytic activity of this enzyme. Substitution of this heterocycle with a carbocycle of similar size but no hydrogen bonding groups (compounds **6f** vs. **4a**) does not preserve the inhibitory potency even when this ring was converted to a warhead for covalent binding.

We also observed that the activity of compounds with Michael acceptor warheads (e.g., **6a** and **6h**) was not improved over the non-covalent inhibitor. This was not unexpected as the catalytic cysteine is near

the carbon of the imidazole adjacent to the carbonyl in **4a** (crystal structure, Figure 2), while a conjugate addition requires making a bond with the more distant carbon atom which would not interact with the oxy-anion hole as does the imidazole ring. However, a more reactive and flexible Michael acceptor warhead (**6i**) led to a significant improvement of the potency. In contrast, the ketoamide **6m**, a warhead which fulfills these geometrical restrictions, does not exhibit a significant increase in potency, although this may be expected because the Michael acceptors would act as irreversible inhibitors while the ketoamide is more likely a reversible inhibitor. We further selected a Michael acceptor warhead (**6l**) which would properly position the reactive carbon next to the catalytic cysteine. Unfortunately, this strategy did not improve the potency and the irreversible α-chloro amide and vinyl sulfonamide derivatives remained the most potent.

As shown in Figure 2, a water molecule (HOH518) interacts with the inhibitor imidazole and the catalytic His^{41}. However, as this water is in a hydrophobic pocket (Val^{42}, Thr^{25}, Leu^{27}), removing this interaction with the water molecule may be detrimental to the free energy of binding due to desolvation penalty. A water molecule in the same location is observed with **4b** (PDB code: 3V3M) although not interacting with the inhibitor and with some of the pseudo peptidic inhibitors such as in structure PDB code: 6Y2G. In an attempt to displace or interact with this water molecule, longer covalent groups were designed (e.g., **6l**). Unfortunately, this only led to loss of potency.

Covalent binding. To evaluate the covalent inhibition hypothesis, we measured the time dependence of the inhibition of our most potent inhibitor, **6k**. As can be seen in Figure 6, the level of inhibition increases over time when the inhibitor is used close to its IC_{50} concentration, while it remains constant for the non-covalent inhibitor **4a**. This observation is consistent with the slow formation of a covalent adduct. Furthermore, the presence of the 3CL^{pro}-**6k** and 3CL^{pro}-**6i** adducts were confirmed by LC-MS (Figures S3 and S4). When the protease was incubated with inhibitor **6k**, the population of unmodified protein decreases as a new population with mass of the protease-inhibitor complex (3CL^{pro} + **6k**) appears, persists while denaturation occurs (Figure S3).

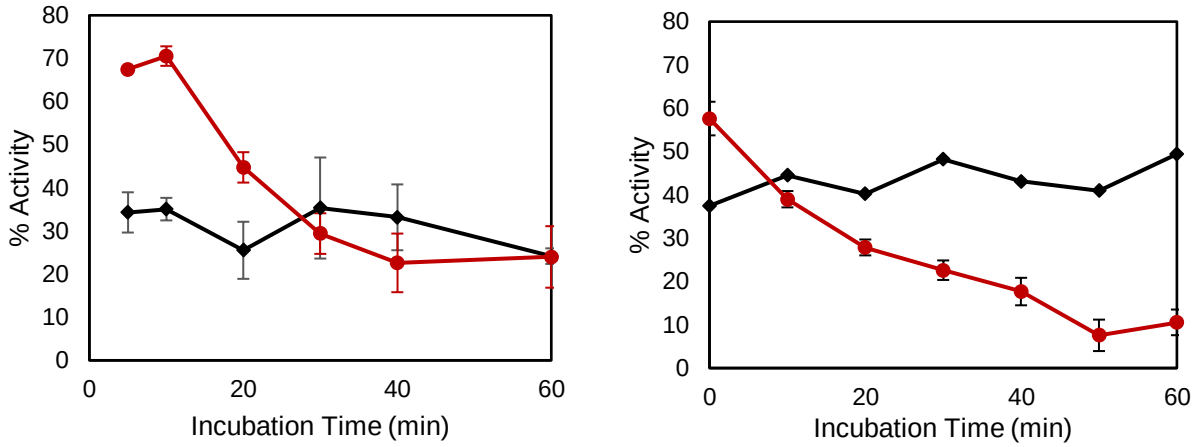

Figure 6. Time-dependent potency for **4a** (black) and **6k** (left, red) and **6i** (right, red).

As a definite proof of covalent inhibition and mode of binding, a crystal structure of 3CL^{pro} co-crystallized with **6k** was obtained. This validates the model proposed at the outset of this project (Figure 7). As can be seen from Figure 7, the constraint resulting from the covalent bond led to the inhibitor being slightly shifted to the left relative to **4a**. This translation resulted in the loss of a hydrogen bond with the backbone amide of Glu^{166}. We believe that increasing the length of the warhead (from **6k** to **6i**) should translate the inhibitor back to the position of 4a and restore this hydrogen bond. Efforts are ongoing to obtain a crystal structure with **6i**.

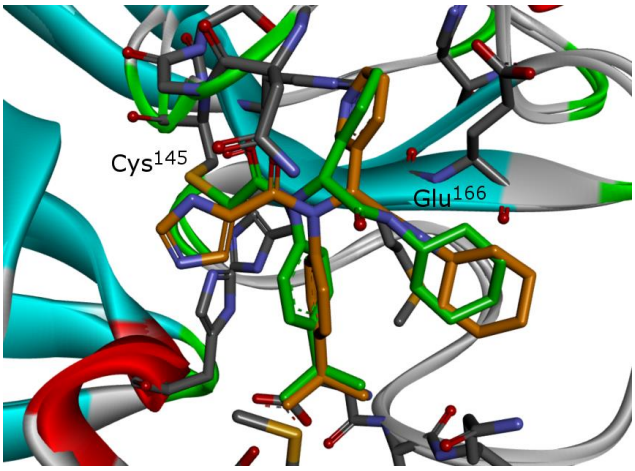

Figure 7. Crystal structure of **6k** (green) bound to 3CL^{pro} overlaid with **4a** (orange) bound to 3CL^{pro} (6W63)

Isothermal Titration Calorimetry (ITC). ITC was employed to validate the initial fluorescence inhibition assay. ITC provides unique insights into the kinetics and thermodynamics of inhibitor binding that are not available in traditional enzyme assays.[43] ITC experiments measure the heat flow or power produced by catalysis as a function of time (Figure 8, y- and *x*-axis, respectively), as one component is titrated into another. The power is proportional to the enzyme velocity, with larger deflections corresponding to higher velocities. Exothermic and endothermic reactions giving downward and upward deflections of the ITC signal, respectively. Since the instrument detects the heat released by the native reaction, unlabeled substrates can be used in the experiments, unlike the fluorescence assay which requires substrates modified with large hydrophobic dyes and quenchers.

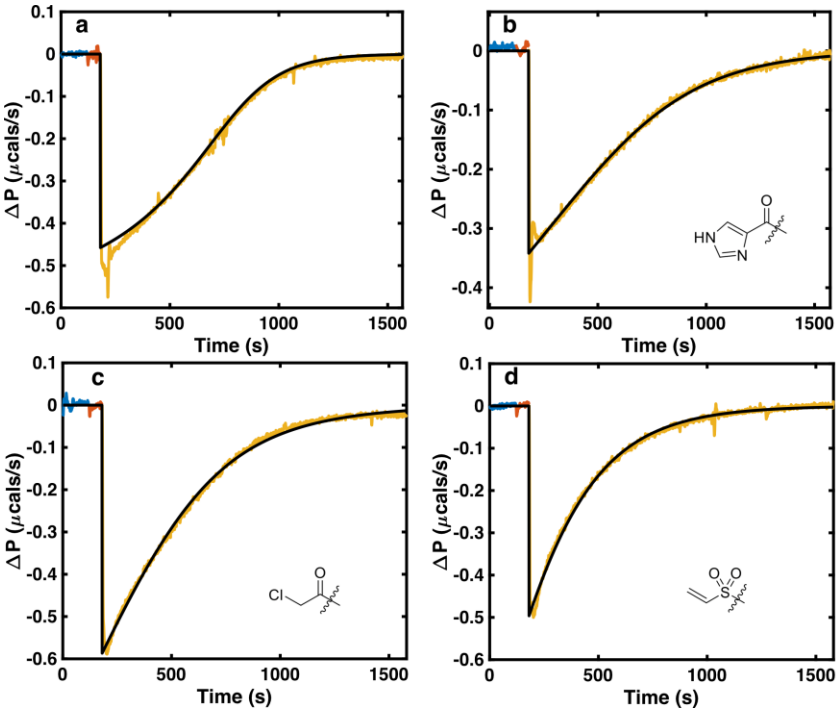

Figure 8. ITC enzyme activity assay in the presence of a) no inhibitor, b) 4.1 µM **4a**, c) 6.4 µM **6k**, d) 6.4 µM **6i** each successive injection is shown in separate color, while ITC simulations corresponding to the minimized kinetic parameters are shown as black.

We performed activity assays where 3CL^{pro} was titrated into the ITC cell, which contained either substrate alone or a mixture of substrate and inhibitor. We then fit the resulting kinetic traces to determine both the mode of inhibition and the kinetic constants of the reactions (i.e., covalent bond formation). First, we extracted Michaelis Menten parameters for the cleavage of the peptide using the ITC trace seen in Figure 8a, as described in the supplementary information. A competitive inhibition model was fit to the ITC traces containing inhibitor, good agreement was found for compound **4a** however, both **6k** and **6i** had

poor agreement with experimental data (Supplementary Figure 5). Instead these traces were fit to a covalent inhibition model using the Michaelis Menten parameters found from fitting the ITC traces for substrate and enzyme alone. These fits gave on-rates for both **6k** and **6i**, which were found to be 657 M^{-1} s^{-1} and 1360 M^{-1} s^{-1} respectively. Under the conditions used during the time-dependent potency experiments seen in Figure 6 these on rates would predict a $t_{1/2}$ of 44 minutes for **6k** and 16 minutes for **6i**. While these values are slower than what is seen during the time-dependent potency experiments, they do show that **6i** has faster kinetics than **6k** and further support the hypothesis that both of these compounds are binding covalently to 3CL^{pro}.

Structure-Activity Relationship. Following our search for an optimal warhead, several modifications were made to the core of the molecule (Tables 2, 3 and 4). Previously, it was shown that replacement of the *t*BuPh group (R^3) by smaller groups or differently substituted phenyl groups modulates the potency against SARS-CoV 3CL^{pro} with slight improvements in some cases, while various hydrophobic groups were tolerated as R^2.[41] We thought this information could help further improve these inhibitors for the highly homologous SARS-CoV-2 3CL^{pro}. However, any attempt to improve the side groups has proven unsuccessful to date; a single modification (**8h**) led to a compound equipotent to **6k**.

Table 2. Inhibitory potency against SARS-CoV-2 3CL^{pro}. Optimization of R^2.

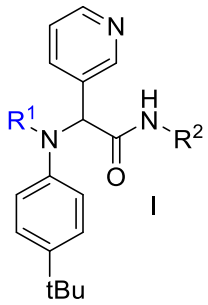

I

Entry	Scaffold	Cmpd	R^1	R^2	Inhibition (%)[a]	IC_{50} (μM) (K_i)
1	I	**8a**	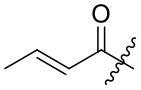	tBu	33 ± 1	nd[b]
2	I	**8b**	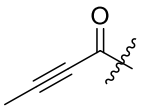	tBu	93	15.0 ± 9.3

3	I	**8c**	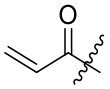	tBu	68 ± 1	nd[b]
4	I	**8d**		tBu	< 5	nd[b]
5	I	**8e**	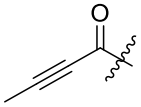	cPent	> 95	1.17 ± 0.26
6	I	**8f**	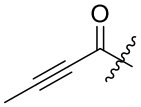	Bn	93± 1	9.5 ± 0.9
7	I	**8g**	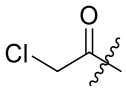	cPent	> 95	1.07 ± 0.65
8	I	**8h**	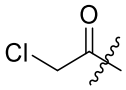	Bn	> 95	0.38 ± 0.09 (0.15 ± 0.05)
9	I	**8i**	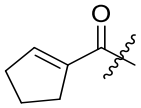	cPent	16	nd[b]

[a] The enzyme activity was measured with 150nM 3CL^{pro} (114 nM after inhibitor addition) and 50 μM of each potential inhibitor with incubation time of 30 min. [b] not determined. *Ki* determined with Km=14 μM, [E] = 0.12 μM and [S] = 11.8 μM.

Table 3. Inhibitory potency against SARS-CoV-2 3CL^{pro}. Optimization of R^4.

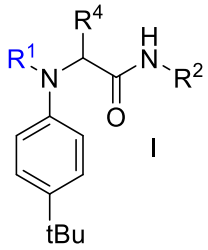

Entry	Scaffold	Cmpd	R^1	R^2	R^4	Inhibition (%)[a]	IC$_{50}$ (μM)
1	I	**9a**	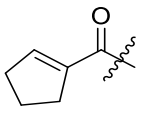	cHex	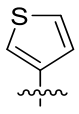	22 ± 8	nd[b]

2	I	**9b**	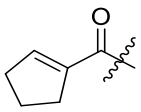	cHex	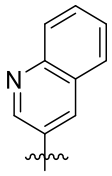	18 ± 8	nd[b]
3	I	**9c**	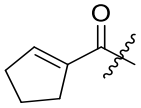	cHex	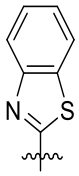	< 5	nd[b]
4	I	**9d**	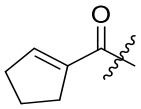	cHex	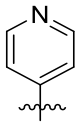	19 ± 8	nd[b]
5	I	**9e**	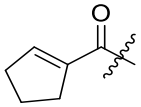	cHex	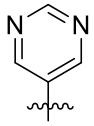	38 ± 8	nd[b]
6	I	**9f**	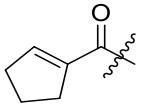	cHex	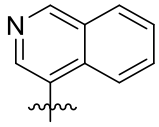	< 5	nd[b]
7	I	**9g**	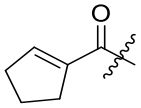	cHex	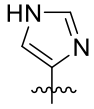	24 ± 8	nd[b]
8	I	**9h**	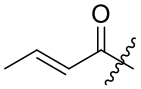	tBu	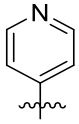	24 ± 8	nd[b]
9	I	**9i**	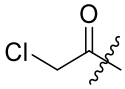	cHex		22 ± 11	nd[b]
10	I	**9j**	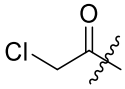	cHex	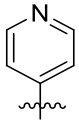	91 ± 1	0.91 ± 0.12
11	I	**9k**	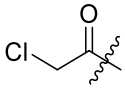	cHex	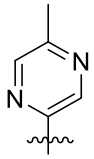	80 ± 4	15 ± 5
12	I	**9l**	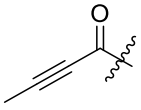	cHex	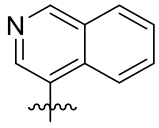	> 95	5.0 ± 2.3

13	I	**9m**	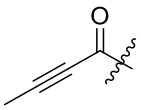	cHex	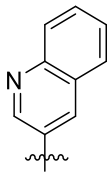	80 ± 10	nd[b]
14	I	**9n**	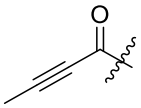	cHex	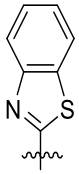	54 ± 15	nd[b]
15	I	**9o**	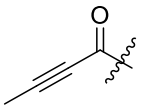	cHex	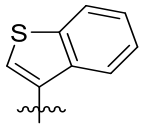	57 ± 6	nd[b]

[a] The enzyme activity was measured with 150 nM 3CL^{pro} (114 nM after inhibitor addition) and 50 μM of each potential inhibitor with incubation time of 30 min. [b] not determined.

Table 4. Inhibitory potency against SARS-CoV-2 3CL^{pro}. Optimization of R^3.

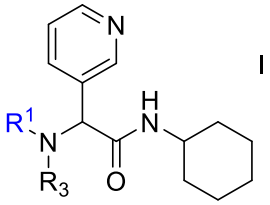

Entry	Scaffold	Cmpd	R^1	R^3	Inhibition (%)[a]	IC$_{50}$ (μM)
1	I	**10a**	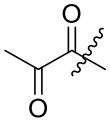	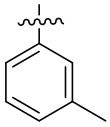	< 5%	nd[b]
2	I	**10b**	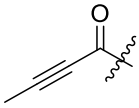	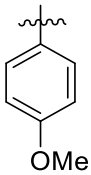	39 ± 1	nd[b]
3		**10c**	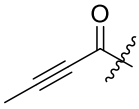	-H	10 ± 15	nd[b]
4		**10d**	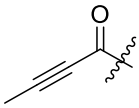	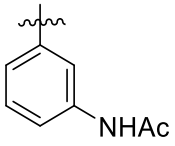	43 ± 3	nd[b]

5	**10e**	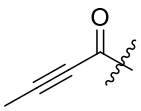	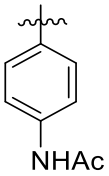	23 ± 13	nd[b]
6	**10f**	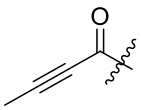	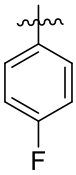	65 ± 3	nd[b]
7	**10g**	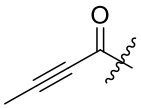	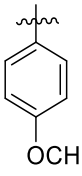	77 ± 2	45.1 ± 18.3

[a] The enzyme activity was measured with 150 nM 3CL^{pro} (114 nM after inhibitor addition) and 50 μM of each potential inhibitor with incubation time of 30 min. [b] not determined.

Conclusion

Covalent inhibition of SARS-CoV-2 3CL^{pro} is a promising strategy for the treatment of COVID-19. Our strategy relied on a previously reported imidazole-containing inhibitor of the similar coronavirus SARS-CoV responsible for the epidemic of SARS in the early 2000's. We first used our docking program FITTED, specifically modified to accommodate covalent inhibitors, and screened a set of covalent warheads. The docked poses confirmed that replacing the imidazole ring by a reactive group should lead to potent covalent inhibition. Gratifyingly, while the imidazole of **4a** was known to be essential for the inhibitory potency, replacing it with many warheads maintained and even improved the potency, with our lead compounds **6k** and **6i** being an order of magnitude more potent. Both, the inhibition pattern of enzymatic activity and the biophysical data first suggested that these inhibitors bind covalently to the viral protease, a binding mode later confirmed by crystallography; thus, the robustness of *in silico* rational-drug design was validated using *in vitro* detection of protein processing.

Experimental section

Synthesis and characterization

General Considerations. All other reagents were purchased from commercial suppliers and used without further purification. All ^{1}H and ^{13}C NMR spectra were acquired Bruker Avance 500 MHz spectrometer. Chemical shifts are reported in ppm using the residual of deuterated solvents as an internal standard. Chromatography was performed on silica gel 60 (230-40 mesh) or using the Biotage One Isolera with ZIP cartridges. High resolution mass spectrometry was performed by ESI on a Bruker Maxis Impact API QqTOF mass spectrometer at McGill University.

General Procedure for 4-Component Ugi Reaction. In a 6-dram vial equipped with a stir bar aldehyde (1.0 mmol, 1.0 eq.), aniline (1.0 mmol, 1.0 eq.) and carboxylic acid (1.0 mmol, 1.0 eq.) were combined in MeOH (4 mL). The obtained reaction mixture was stirred for 30 min at room temperature. Afterwards cyclohexyl isocyanide (0.9 mmol, 0.9 eq.) was added to the reaction mixture and the walls of the vial were washed with 1 mL of MeOH. The reaction mixture was continued to stir at room temperature overnight. The crude reaction mixture was evaporated in vacuo. Purification procedure A) The crude product was triturated with hexanes (5 mL) and filtered. The obtained product was further washed with hexanes (3 x 3 mL). Purification procedure B) The crude product recrystallized from $CHCl_3$/Hexanes mixture, filtered and the obtained product was further washed with hexanes (3 x 3 mL). Purification procedure C) The crude product was redissolved in DCM. The obtained crude solution was deposited on silica. It was then purified using flash column chromatography using DCM/MeOH (gradient 0 → 5%) as eluent.

***N*-(4-(*tert*-butyl)phenyl)-*N*-(2-(cyclohexylamino)-2-oxo-1-(pyridin-3-yl)ethyl)-1*H*-imidazole-5-carboxamide (4a).** ^{1}H NMR (500 MHz, MeOD) δ 8.37 (s, 1H), 8.33 (dd, *J* = 4.9, 1.5 Hz, 1H), 7.66 – 7.57 (m, 2H), 7.31 (d, *J* = 7.8 Hz, 2H), 7.22 (dd, J = 7.9, 4.9 Hz, 1H), 6.27 (s, 1H), 5.46 (s, 1H), 3.71 (td, *J* = 10.5, 9.3, 3.9 Hz, 1H), 1.93 (d, *J* = 12.3 Hz, 1H), 1.80 – 1.72 (m, 2H), 1.65 (ddt, *J* = 30.9, 12.9, 3.8 Hz, 2H), 1.27 (s, 12H). ^{13}C NMR (126 MHz, MeOD) δ 169.00, 152.54, 150.62, 148.24, 138.83, 136.36, 131.58, 131.07, 125.72, 123.31, 62.74, 34.16, 32.16, 32.12, 30.25, 25.22, 24.72, 24.64. HRMS (ESI/Q-TOF) m/z: $[M + Na]^+$ calculated for $C_{27}H_{33}N_5NaO_2$ 482.2526; found 482.2535.

***N*-(4-(*tert*-butyl)phenyl)-*N*-(2-(*tert*-butylamino)-2-oxo-1-(pyridin-3-yl)ethyl)furan-2-carboxamide (4b).** Compound was purified using general procedure A, white solid 84 % yield, 290 mg. ^{1}H NMR (500 MHz, $CDCl_3$) δ 8.48 (d, *J* = 2.3 Hz, 1H), 8.46 (dd, *J* = 4.9, 1.7 Hz, 1H), 7.51 (d, *J* = 8.1 Hz, 1H), 7.39 (dd, *J* = 1.7, 0.7 Hz, 1H), 7.24 (d, *J* = 6.6 Hz, 2H), 7.06 (ddd, *J* = 8.0, 4.8, 0.8 Hz, 1H), 6.98 (s, 2H), 6.19 – 6.13 (m, 2H), 6.10 (s, 1H), 5.38 (dd, *J* = 3.6, 0.8 Hz, 1H), 1.37 (s, 9H), 1.28 (s, 9H). ^{13}C

NMR (126 MHz, $CDCl_3$) δ 167.96, 159.80, 152.62, 151.59, 149.72, 146.36, 145.12, 138.32, 136.63, 130.56, 130.30, 126.22, 122.94, 117.26, 111.35, 63.83, 51.92, 34.84, 31.41, 28.80. HRMS (ESI/Q-TOF) m/z: $[M + Na]^+$ calculated for $C_{26}H_{31}N_3NaO_3$ 456.2258; found 456.2245.

2-(*N*-(4-(*tert*-butyl)phenyl)acetamido)-*N*-cyclohexyl-2-(pyridin-3-yl)acetamide (5a). Compound was purified using general procedure A, white solid 76 % yield, 280 mg. ^{1}H NMR (500 MHz, $CDCl_3$) δ 8.46 – 8.43 (m, 1H), 8.42 (s, 1H), 7.41 (d, *J* = 8.1 Hz, 1H), 7.23 (d, *J* = 8.5 Hz, 2H), 7.03 (dd, *J* = 8.0, 4.8 Hz, 1H), 6.93 (s, 1H), 6.03 (s, 2H), 3.94 – 3.65 (m, 1H), 1.98 (d, *J* = 16.8 Hz, 1H), 1.89 – 1.81 (m, 4H), 1.75 – 1.63 (m, 2H), 1.59 (dt, *J* = 13.0, 4.3 Hz, 1H), 1.43 – 1.28 (m, 2H), 1.25 (s, 9H), 1.23 – 1.04 (m, 3H). ^{13}C NMR (126 MHz, $CDCl_3$) δ 171.83, 168.21, 151.89, 151.44, 149.66, 138.09, 137.42, 130.87, 129.60, 126.28, 122.92, 62.42, 48.88, 34.73, 32.95 (d, *J* = 10.4 Hz), 31.37, 25.61, 24.87 (d, *J* = 6.9 Hz), 23.34. HRMS (ESI/Q-TOF) m/z: $[M + Na]^+$ calculated for $C_{25}H_{33}N_3NaO_2$ 430.2465; found 430.2464.

***N*-cyclohexyl-2-(pyridin-3-yl)-2-(*p*-tolylamino)acetamide (5b).** To a solution of 4-*t*Bu-aniline (1.01 mmol, 0.16 mL) and 3-pyridinecarboxaldehyde (1.01 mmol, 0.09 mL) in MeOH (5 mL) was added cyclohexyl isocyanide (1.01 mmol, 0.12 mL) and phosphoric acid (0.2 mmol, 0.01 mL, 85%), and the solution stirred at room temperature overnight. The solvent was evaporated under a stream of air, and the crude reaction mixture was suspended in a small amount of EtOAc. Hexanes was added and the precipitate was collected by filtration and rinsed with hexanes and acetone. The precipitate was dried over vacuum to afford the desired product (353 mg, 96% yield) as a white powder. ^{1}H NMR (500 MHz, DMSO) δ 8.69 (dd, *J* = 2.4, 0.9 Hz, 1H), 8.46 (dd, *J* = 4.8, 1.7 Hz, 1H), 8.19 (d, *J* = 7.9 Hz, 1H), 7.85 (dt, *J* = 7.9, 2.0 Hz, 1H), 7.35 (ddd, *J* = 7.8, 4.8, 0.9 Hz, 1H), 7.10 – 7.04 (m, 2H), 6.61 – 6.55 (m, 2H), 6.04 (d, *J* = 8.1 Hz, 1H), 5.02 (d, *J* = 8.0 Hz, 1H), 3.56 – 3.47 (m, 1H), 1.74 (dd, *J* = 10.5, 4.8 Hz, 1H), 1.70 – 1.63 (m, 1H), 1.62 – 1.48 (m, 3H), 1.31 – 1.19 (m, 2H), 1.18 (s, 10H), 1.17 – 1.03 (m, 1H). ^{13}C NMR (126 MHz, DMSO) δ 169.29, 148.65, 148.56, 144.47, 138.99, 135.44, 134.52, 125.39, 123.45, 112.89, 58.39, 47.58, 33.46, 32.24, 32.06, 31.38, 25.11, 24.37, 24.26. HRMS (ESI/Q-TOF) m/z: $[M + Na]^+$ calculated for C23H31N3NaO 388.2359; found 388.2352.

***N*-(4-(*tert*-butyl)phenyl)-*N*-(2-(cyclohexylamino)-2-oxo-1-(pyridin-3-yl)ethyl) acrylamide (6a).** Compound was purified using general procedure C, white solid 32 % yield, 120 mg. ^{1}H NMR (500 MHz, $CDCl_3$) δ 8.41 – 8.39 (m, 1H), 8.38 – 8.37 (m, 1H), 7.42 – 7.35 (m, 1H), 7.19 (d, *J* = 8.1 Hz, 2H), 7.01 (dd, *J* = 8.0, 4.8 Hz, 1H), 6.91 (s, 1H), 6.49 (d, *J* = 8.0 Hz, 1H), 6.33 (dd, *J* = 16.8, 2.0 Hz, 1H), 6.11 (s, 1H), 5.93 (dd, *J* = 16.8, 10.3 Hz, 1H), 5.49 (dd, *J* = 10.4, 2.0 Hz, 1H), 3.84 – 3.73 (m, 1H), 1.93 (s, 1H),

1.81 (dd, *J* = 13.1, 4.1 Hz, 1H), 1.67 – 1.53 (m, 3H), 1.37 – 1.26 (m, 2H), 1.22 (s, 9H), 1.17 – 1.06 (m, 3H). ^{13}C NMR (126 MHz, $CDCl_3$) δ 168.04, 166.50, 151.79, 151.28, 149.45, 137.93, 136.14, 130.83, 129.93, 128.64, 128.52, 126.08, 122.85, 62.69, 48.76, 34.64, 32.86, 32.80, 31.27, 25.52, 24.83, 24.77. HRMS (ESI/Q-TOF) m/z: $[M + Na]^+$ calculated for $C_{26}H_{33}N_3NaO_2$ 442.2465; found 442.2456.

***N*-(4-(*tert*-butyl)phenyl)-*N*-(2-(cyclohexylamino)-2-oxo-1-(pyridin-3-yl)ethyl) cinnamamide (6b).** Compound was purified using general procedure A, pale white solid 94 % yield, 420 mg. ^{1}H NMR (500 MHz, $CDCl_3$) δ 8.48 (d, *J* = 2.3 Hz, 1H), 8.47 (dd, *J* = 4.8, 1.7 Hz, 1H), 7.71 (d, *J* = 15.6 Hz, 1H), 7.50 (dt, *J* = 7.9, 2.0 Hz, 1H), 7.27 (s, 6H), 7.07 (dd, *J* = 8.0, 4.8 Hz, 1H), 6.98 (s, 1H), 6.33 (d, *J* = 8.1 Hz, 1H), 6.24 (d, *J* = 15.5 Hz, 1H), 6.14 (s, 1H), 3.91 – 3.80 (m, 1H), 1.94 (dd, *J* = 52.0, 13.0 Hz, 2H), 1.70 (ddd, *J* = 18.3, 11.4, 6.7 Hz, 2H), 1.59 (dd, *J* = 8.9, 4.1 Hz, 1H), 1.44 – 1.32 (m, 2H), 1.29 (s, 9H), 1.26 – 1.09 (m, 4H). ^{13}C NMR (126 MHz, CDCl3) δ 168.16, 167.14, 151.97, 151.36, 149.60, 143.22, 138.03, 136.60, 135.07, 130.93, 129.91, 129.86, 128.82, 128.13, 126.35, 122.95, 118.61, 63.32, 48.85, 34.81, 33.02, 32.96, 31.38, 25.62, 24.90, 24.86. HRMS (ESI/Q-TOF) m/z: $[M + Na]^+$ calculated for $C_{32}H_{37}N_3NaO_2$ 518.2778; found 518.2790.

(*E*)-*N*-(4-(*tert*-butyl)phenyl)-*N*-(2-(cyclohexylamino)-2-oxo-1-(pyridin-3-yl)ethyl)but-2-enamide (6c). Compound was purified using general procedure B, pale white solid 32 % yield, 126 mg. ^{1}H NMR (500 MHz, CDCl3) δ 8.46 – 8.41 (m, 2H), 7.44 (dt, J = 7.9, 2.0 Hz, 1H), 7.24 (d, J = 8.2 Hz, 2H), 7.04 (ddd, J = 8.0, 4.8, 0.8 Hz, 1H), 6.99 – 6.91 (m, 3H), 6.36 (d, J = 8.1 Hz, 1H), 6.09 (s, 1H), 5.65 (dd, J = 15.0, 1.7 Hz, 1H), 3.87 – 3.76 (m, 1H), 1.97 (dd, J = 11.7, 4.6 Hz, 1H), 1.92 – 1.82 (m, 1H), 1.72 (dd, J = 7.0, 1.7 Hz, 3H), 1.69 – 1.63 (m, 1H), 1.60 – 1.56 (m, 1H), 1.42 – 1.30 (m, 2H), 1.27 (s, 9H), 1.22 – 1.09 (m, 3H). ^{13}C NMR (126 MHz, $CDCl_3$) δ 168.25, 166.99, 151.78, 151.24, 149.41, 143.08, 138.09, 136.62, 131.00, 129.80, 126.22, 122.88, 122.71, 62.96, 48.78, 34.75, 32.97, 32.91, 31.37, 25.62, 24.88, 24.84, 18.21. HRMS (ESI/Q-TOF) m/z: $[M + Na]^+$ calculated for $C_{27}H_{35}N_3NaO_2$ 456.2621; found 456.2630.

(*E*)-*N*-(4-(*tert*-butyl)phenyl)-*N*-(2-(cyclohexylamino)-2-oxo-1-(pyridin-3-yl)ethyl)-2-methylbut-2-enamide (6d). Compound was purified using general procedure A, white solid 73 % yield, 294 mg. ^{1}H NMR (500 MHz, $CDCl_3$) δ 8.50 (d, *J* = 2.3 Hz, 1H), 8.49 – 8.45 (m, 1H), 7.55 (dt, *J* = 7.9, 2.0 Hz, 1H), 7.17 (d, *J* = 8.8 Hz, 2H), 7.10 (ddd, *J* = 7.9, 4.8, 0.8 Hz, 1H), 6.87 (d, *J* = 8.1 Hz, 2H), 6.29 (d, *J* = 8.2 Hz, 1H), 5.98 (s, 1H), 5.77 (dddd, *J* = 8.5, 6.9, 5.5, 1.6 Hz, 1H), 3.90 – 3.79 (m, 1H), 1.96 (d, *J* = 9.1 Hz, 1H), 1.92 – 1.87 (m, 1H), 1.74 – 1.55 (m, 3H), 1.51 (s, 3H), 1.45 (dd, *J* = 6.9, 1.2 Hz, 3H), 1.44 – 1.30 (m, 2H), 1.24 (s, 9H), 1.23 – 1.08 (m, 3H). ^{13}C NMR (126 MHz, $CDCl_3$) δ 174.17, 168.17, 151.06, 150.92, 149.49,

138.40, 137.72, 132.44, 131.30, 131.17, 128.98, 125.80, 123.03, 64.28, 34.67, 33.00, 32.98, 31.36, 25.63, 24.86, 24.81, 14.17, 13.46. HRMS (ESI/Q-TOF) m/z: $[M + Na]^+$ calculated for $C_{28}H_{37}N_3NaO_2$ 470.2778; found 470.2766.

***N*-(4-(*tert*-butyl)phenyl)-*N*-(2-(cyclohexylamino)-2-oxo-1-(pyridin-3-yl)ethyl) methacrylamide (6e)**. Compound was purified using general procedure B, pale white solid 68 % yield, 265 mg. ^{1}H NMR (500 MHz, MeOD) δ 8.33 (d, *J* = 2.3 Hz, 1H), 8.31 (dd, *J* = 4.9, 1.6 Hz, 1H), 7.56 (dt, *J* = 7.9, 2.0 Hz, 1H), 7.23 – 7.15 (m, 3H), 7.05 (s, 2H), 6.10 (s, 1H), 5.01 (dt, *J* = 6.9, 1.3 Hz, 2H), 3.70 (tt, *J* = 10.9, 3.9 Hz, 1H), 1.90 (dd, *J* = 10.7, 3.8 Hz, 1H), 1.73 (s, 5H), 1.70 – 1.59 (m, 2H), 1.41 – 1.27 (m, 3H), 1.21 (s, 9H), 1.19 – 1.06 (m, 2H). ^{13}C NMR (126 MHz, $CDCl_3$) δ 172.82, 167.95, 151.29, 151.19, 149.55, 140.42, 137.86, 137.64, 130.88, 129.32, 125.77, 122.97, 119.77, 63.47, 48.78, 34.63, 32.90 (d, *J* = 10.4 Hz),, 31.32, 25.57, 24.83, 24.77, 20.42. HRMS (ESI/Q-TOF) m/z: $[M + Na]^+$ calculated for $C_{27}H_{35}N_3NaO_2$ 456.2621; found 456.2620.

***N*-(4-(*tert*-butyl)phenyl)-*N*-(2-(cyclohexylamino)-2-oxo-1-(pyridin-3-yl)ethyl)cyclopent-1-ene-1-carboxamide (6f).** Compound was purified using general procedure A, pale yellow solid 80 % yield, 333 mg. ^{1}H NMR (500 MHz, CDCl3) δ 8.48 (d, J = 2.3 Hz, 1H), 8.46 (dd, J = 4.8, 1.7 Hz, 1H), 7.51 (dt, J = 8.0, 2.0 Hz, 1H), 7.21 – 7.16 (m, 2H), 7.08 (ddd, J = 7.9, 4.8, 0.8 Hz, 1H), 6.90 (d, J = 8.0 Hz, 2H), 6.28 (d, J = 8.0 Hz, 1H), 6.04 (s, 1H), 5.82 (d, J = 2.3 Hz, 1H), 3.89 – 3.78 (m, 1H), 2.19 (ddt, J = 7.7, 5.1, 2.5 Hz, 2H), 2.12 (tt, J = 6.7, 2.8 Hz, 2H), 2.02 – 1.93 (m, 1H), 1.92 – 1.84 (m, 1H), 1.73 – 1.54 (m, 4H), 1.44 – 1.29 (m, 2H), 1.25 (s, 9H), 1.23 – 1.07 (m, 3H). ^{13}C NMR (126 MHz, CDCl3) δ 168.92, 168.16, 151.57, 151.22, 149.46, 140.13, 139.09, 137.96, 137.69, 130.98, 129.50, 125.81, 122.94, 63.92, 48.74, 34.69, 33.80, 33.22, 32.95, 32.92, 31.35, 25.60, 24.84, 24.79, 23.29. HRMS (ESI/Q-TOF) m/z: $[M + Na]^+$ calculated for $C_{29}H_{37}N_3NaO_2$ 482.2778; found 482.2781.

***N*-(4-(*tert*-butyl)phenyl)-*N*-(2-(cyclohexylamino)-2-oxo-1-(pyridin-3-yl)ethyl)cyclohex-1-ene-1-carboxamide (6g).** Compound was purified using general procedure A, white solid 37 % yield, 157 mg. ^{1}H NMR (500 MHz, $CDCl_3$) δ 8.50 (d, *J* = 2.3 Hz, 1H), 8.47 (dd, *J* = 4.8, 1.6 Hz, 1H), 7.55 (dt, *J* = 8.0, 2.0 Hz, 1H), 7.18 (d, *J* = 8.8 Hz, 2H), 7.11 (ddd, *J* = 7.9, 4.8, 0.8 Hz, 1H), 6.88 (d, *J* = 8.1 Hz, 2H), 6.30 (d, *J* = 8.2 Hz, 1H), 6.00 (s, 1H), 5.84 (dt, *J* = 3.8, 2.0 Hz, 1H), 3.90 – 3.79 (m, 1H), 1.99 – 1.80 (m, 5H), 1.75 – 1.54 (m, 6H), 1.44 – 1.29 (m, 4H), 1.25 (s, 9H), 1.24 – 1.13 (m, 3H). ^{13}C NMR (126 MHz, $CDCl_3$) δ 173.52, 168.18, 151.11, 151.05, 149.50, 138.33, 137.79, 134.48, 133.17, 131.12, 129.08, 125.69, 123.02,

63.95, 48.72, 34.68, 33.01, 32.97, 31.37, 26.14, 25.64, 25.00, 24.85, 22.04, 21.45. HRMS (ESI/Q-TOF) m/z: $[M + Na]^+$ calculated for $C_{30}H_{39}N_3NaO_2$ 496.2934; found 496.2931.

***N*-(4-(*tert*-butyl)phenyl)-*N*-(2-(cyclohexylamino)-2-oxo-1-(pyridin-3-yl)ethyl)but-2-ynamide (6h).** Compound was purified using general procedure A, white solid 92 % yield, 357 mg. ^{1}H NMR (500 MHz, $CDCl_3$) δ 8.44 (d, *J* = 4.9 Hz, 1H), 8.41 (d, *J* = 2.3 Hz, 1H), 7.44 (d, *J* = 8.1 Hz, 1H), 7.21 (d, *J* = 8.4 Hz, 2H), 7.05 (dd, *J* = 8.0, 4.8 Hz, 1H), 6.97 (d, *J* = 8.0 Hz, 2H), 6.20 (s, 1H), 6.03 (s, 1H), 3.80 (dtd, *J* = 10.8, 7.2, 4.0 Hz, 1H), 1.96 (dq, *J* = 13.2, 4.8 Hz, 1H), 1.84 (d, *J* = 16.6 Hz, 1H), 1.75 – 1.62 (m, 5H), 1.58 (dd, *J* = 13.1, 4.1 Hz, 1H), 1.42 – 1.26 (m, 2H), 1.25 (s, 9H), 1.25 – 1.05 (m, 3H). ^{13}C NMR (126 MHz, $CDCl_3$) δ 167.43, 155.41, 151.87, 151.20, 149.62, 138.15, 136.38, 130.34, 129.90, 125.70, 122.98, 92.12, 73.86, 62.23, 34.71, 32.87, 32.80, 31.31, 25.56, 24.85, 24.80. HRMS (ESI/Q-TOF) m/z: $[M + Na]^+$ calculated for $C_{27}H_{33}N_3NaO_2$ 454.2465; found 454.2458.

***N*-cyclohexyl-2-(pyridin-3-yl)-2-(*p*-tolylamino)acetamide (6i).** To a solution of **7** (0.41 mmol, 150 mg) in DCM (4 mL) was added pyridine (0.56 mmol, 0.04 mL) and the solution cooled to 0ºC. 2-chloroethanesulfonyl chloride (0.49 mmol, 0.05 mL) was added dropwise and stirred for 1h, after which pyridine (0.56 mmol, 0.04 mL) was added, and the solution was warmed to r.t. and stirred overnight. The reaction was monitored by TLC (1:1 DCM:EA). The reaction was quenched with water and extracted with DCM (x2). The combined organic layers were washed with sat. NH4Cl, sat. $NaHCO_3$ and brine, dried over Na_2SO4, and concentrated in vacuo. The crude product was further purified by column chromatography (0-4% (MeOH+1%NH4OH)/DCM) to afford the pure product (66 mg, 35% yield) as a white powder. ^{1}H NMR (500 MHz, DMSO) δ 8.35 (dd, *J* = 4.9, 1.6 Hz, 1H), 8.31 (s, 0H), 8.10 (d, *J* = 7.6 Hz, 1H), 7.36 (dt, *J* = 8.0, 2.0 Hz, 1H), 7.17 – 7.09 (m, 4H), 6.98 (dd, *J* = 16.5, 9.9 Hz, 1H), 6.06 (d, *J* = 9.9 Hz, 1H), 5.98 (d, *J* = 16.5 Hz, 1H), 5.81 (s, 1H), 3.57 (tdt, *J* = 11.0, 7.6, 3.7 Hz, 1H), 1.79 – 1.72 (m, 1H), 1.67 (dt, J = 12.9, 4.0 Hz, 1H), 1.64 – 1.47 (m, 2H), 1.33 – 1.19 (m, 2H), 1.17 (s, 9H), 1.16 – 0.92 (m, 2H). ^{13}C NMR (126 MHz, DMSO) δ 167.43, 150.53, 150.51, 148.97, 136.88, 136.07, 133.56, 131.92, 131.00, 127.18, 124.92, 122.94, 63.05, 47.95, 34.19, 32.07, 31.88, 30.94, 25.09, 24.41, 24.31. HRMS (ESI/Q-TOF) m/z: $[M + Na]^+$ calculated for $C_{25}H_{33}N_3NaO_3S$ 478.2135; found 478.2127.

***N*-(4-(*tert*-butyl)phenyl)-*N*-(2-(cyclohexylamino)-2-oxo-1-(pyridin-3-yl)ethyl)-2-fluoroacetamide (6j).** Compound was purified using general procedure A, pale yellow solid 70 % yield, 270 mg. ^{1}H NMR (500 MHz, $CDCl_3$) δ 8.47 (dd, *J* = 4.9, 1.7 Hz, 1H), 8.43 (d, *J* = 2.3 Hz, 1H), 7.43 (dt, *J* = 7.9, 2.0 Hz, 1H), 7.24 (s, 2H), 7.06 (ddd, *J* = 8.0, 4.8, 0.8 Hz, 1H), 6.04 (s, 1H), 5.87 (d, *J* = 7.8 Hz, 1H), 4.64 (d, *J* =

3.1 Hz, 1H), 4.55 (d, *J* = 3.3 Hz, 1H), 3.86 – 3.75 (m, 1H), 2.02 – 1.95 (m, 1H), 1.89 – 1.81 (m, 1H), 1.74 – 1.55 (m, 3H), 1.44 – 1.28 (m, 2H), 1.25 (s, 9H), 1.22 – 1.02 (m, 3H). ^{13}C NMR (126 MHz, $CDCl_3$) δ 168.05, 167.89, 167.48, 153.00, 151.45, 149.99, 138.13, 133.76, 129.97, 129.82, 126.64, 123.12, 78.70 (d, *J* = 178.1 Hz), 62.38, 49.16, 34.84, 32.94 (d, *J* = 9.3 Hz), 31.31, 25.57, 24.90 (d, *J* = 6.9 Hz). HRMS (ESI/Q-TOF) m/z: $[M + Na]^+$ calculated for $C_{25}H_{32}FN_3NaO_2$ 448.2371; found 448.2366.

***N*-(4-(*tert*-butyl)phenyl)-2-chloro-*N*-(2-(cyclohexylamino)-2-oxo-1-(pyridin-3-yl)ethyl) acetamide (6k).** Compound was purified using general procedure A, yellow solid 93 % yield, 370 mg. ^{1}H NMR (500 MHz, $CDCl_3$) δ 8.47 (dd, *J* = 4.8, 1.6 Hz, 1H), 8.43 (d, *J* = 2.3 Hz, 1H), 7.44 (dt, *J* = 7.9, 2.0 Hz, 1H), 7.26 (s, 3H), 7.07 (ddd, *J* = 7.8, 4.9, 0.8 Hz, 1H), 5.99 (s, 1H), 5.88 (s, 1H), 3.85 (s, 2H), 3.84 – 3.78 (m, 1H), 1.98 (dd, *J* = 12.6, 4.2 Hz, 1H), 1.85 (dd, *J* = 12.6, 4.2 Hz, 1H), 1.74 – 1.63 (m, 2H), 1.59 (dt, *J* = 12.8, 3.8 Hz, 1H), 1.43 – 1.28 (m, 2H), 1.26 (s, 9H), 1.22 – 1.03 (m, 3H). ^{13}C NMR (126 MHz, CDCl3) δ 167.43, 167.42, 152.83, 151.27, 149.75, 138.27, 135.35, 130.28, 129.73, 126.61, 123.16, 63.16, 49.11, 42.58, 34.84, 32.97, 32.90, 31.33, 25.57, 24.91, 24.85. HRMS (ESI/Q-TOF) m/z: $[M + Na]^+$ calculated for $C_{25}H_{32}ClN_3NaO_2$ 464.2075; found 464.2087.

Ethyl (*E*)-4-((4-(*tert*-butyl)phenyl)(2-(cyclohexylamino)-2-oxo-1-(pyridin-3-yl)ethyl)amino)-4-oxobut-2-enoate (6l). Product purified using general procedure A, white powder 52% yield, 170 mg. ^{1}H NMR (500 MHz, $CDCl_3$) δ 8.51 – 8.38 (m, 2H), 7.49 (dt, *J* = 8.1, 2.0 Hz, 1H), 7.23 (d, *J* = 8.1 Hz, 2H), 7.09 (dd, *J* = 8.0, 4.8 Hz, 1H), 6.85 (d, *J* = 15.3 Hz, 1H), 6.72 (d, *J* = 15.3 Hz, 1H), 6.24 (d, *J* = 8.1 Hz, 1H), 6.10 (s, 1H), 4.12 (q, *J* = 7.1 Hz, 2H), 3.80 (dtd, *J* = 10.8, 7.2, 4.0 Hz, 1H), 1.98 – 1.90 (m, 1H), 1.89 – 1.79 (m, 1H), 1.72 – 1.53 (m, 3H), 1.33 (ddd, *J* = 13.0, 10.0, 3.3 Hz, 1H), 1.25 (s, 9H), 1.20 (t, *J* = 7.1 Hz, 3H), 1.10 (ddt, *J* = 23.0, 15.4, 10.8 Hz, 1H). ^{13}C NMR (126 MHz, $CDCl_3$) δ 167.37, 165.46, 165.04, 152.42, 150.54, 148.89, 138.83, 135.41, 133.89, 132.15, 130.95, 129.77, 126.48, 123.26, 63.08, 61.13, 49.00, 34.77, 32.90, 32.84, 31.28, 25.53, 24.86, 24.80, 14.11. HRMS (ESI/Q-TOF) m/z: $[M + Na]^+$ calculated for $C_{29}H_{37}N_3NaO_4$ 514.2676; found 514.2691.

***N*-(4-(*tert*-butyl)phenyl)-*N*-(2-(cyclohexylamino)-2-oxo-1-(pyridin-3-yl)ethyl)-2-oxopropanamide (6m).** To a solution of 4-tert-butylaniline (0.10 mL, 0.67 mmol, 1.0 eq.) in MeOH (2 mL) was added 3-pyridine carboxaldehyde (0.06 mL, 0.67 mmol, 1.0 eq.) and the solution stirred at room temperature for 30 minutes. The solution was cooled to 0 ºC, and pyruvic acid (0.06 mL, 0.80 mmol, 1.2 eq.) and cyclohexyl isocyanide (0.10 mL, 0.80 mmol, 1.2 eq.) were added in quick succession. The solution was slowly warmed to room temperature and stirred overnight. The crude reaction mixture was

evaporated in vacuo and purified by column chromatography (1:1 Hex:EtOAc) to afford the product (105 mg, 36%) as a white powder. ^{1}H NMR (500 MHz, $CDCl_3$) δ 8.69 (s, 1H), 8.56 (s, 1H), 7.84 (d, *J* = 8.0 Hz, 1H), 7.35 (d, *J* = 7.7 Hz, 1H), 7.23 (d, *J* = 8.8 Hz, 2H), 7.03 (d, *J* = 8.1 Hz, 2H), 6.49 (d, *J* = 8.0 Hz, 1H), 6.15 (s, 1H), 3.80 (tdd, *J* = 10.7, 6.7, 4.0 Hz, 1H), 2.19 (s, 3H), 1.97 – 1.79 (m, 2H), 1.69 (ddt, *J* = 17.1, 13.1, 4.0 Hz, 2H), 1.59 (dt, *J* = 12.8, 3.9 Hz, 1H), 1.41 – 1.25 (m, 2H), 1.24 (s, 9H), 1.16 (dtd, *J* = 16.2, 13.6, 12.7, 9.9 Hz, 2H).^{13}C NMR (126 MHz, $CDCl_3$) δ 197.49, 168.14, 166.68, 152.69, 150.19, 148.63, 139.25, 134.15, 130.64, 129.82, 126.29, 123.61, 62.36, 49.22, 34.77, 32.85, 32.81, 31.26, 27.84, 25.51, 24.87, 24.81. HRMS (ESI/Q-TOF) m/z: $[M + Na]^+$ calculated for $C_{26}H_{33}N_3NaO_3$ 458.2412; found 458.2421

Ethyl (4-(*tert*-butyl)phenyl)(2-(cyclohexylamino)-2-oxo-1-(pyridin-3-yl)ethyl)carbamate (6n). To a solution of **7** (0.41 mmol, 150 mg) in DCM (8 mL) was added pyridine (0.82 mmol, 0.06 mL) and the solution was cooled to 0ºC. Ethyl chloroformate (0.49 mmol, 0.05 mL) was added dropwise and stirred at 0ºC for 1h, then room temperature overnight. The reaction was quenched with water and extracted twice with DCM. The combined organic layers were washed with sat. NH_4Cl, sat. NaHCO3 and brine, then dried over Na2SO4 and concentrated in vacuo. The crude residue was further purified by column chromatography (0-80% EtOAc/Hex) to afford the desired product (136 mg, 76% yield) as a white powder. ^{1}H NMR (500 MHz, $CDCl_3$) δ 8.55 (s, 1H), 8.51 – 8.46 (m, 1H), 7.66 (dt, *J* = 8.1, 1.9 Hz, 1H), 7.23 (td, *J* = 6.0, 5.5, 2.3 Hz, 3H), 6.97 (d, *J* = 8.5 Hz, 2H), 6.24 (d, *J* = 8.1 Hz, 1H), 5.72 (s, 1H), 4.15 (qd, *J* = 7.1, 2.7 Hz, 2H), 3.84 (dddd, *J* = 14.5, 10.5, 7.9, 3.9 Hz, 1H), 1.99 – 1.83 (m, 2H), 1.69 (tt, *J* = 12.5, 3.9 Hz, 2H), 1.60 (dt, *J* = 12.9, 3.9 Hz, 1H), 1.43 – 1.30 (m, 2H), 1.26 (s, 9H), 1.22 – 1.08 (m, 6H). ^{13}C NMR (126 MHz, CDCl3) δ 167.76, 156.29, 150.83, 148.98, 147.37, 139.54, 137.15, 132.52, 128.33, 126.00, 123.58, 64.95, 62.65, 48.91, 34.67, 32.97, 32.93, 31.38, 25.57, 24.84, 24.82, 14.64. HRMS (ESI/Q-TOF) m/z: $[M + Na]^+$ calculated for $C_{26}H_{35}N_3NaO_3$ 460.2571; found 460.2579.

2-((4-(*tert*-butyl)phenyl)(cyanomethyl)amino)-N-cyclohexyl-2-(pyridin-3-yl)acetamide (6p). To a solution of 2-((4-(*tert*-butyl)phenyl)amino)acetonitrile (0.27 mmol, 50 mg) and 3-pyridinecarboxaldehyde (0.27 mmol, 0.03 mL) in MeOH (3 mL) was added cyclohexyl isocyanide (0.27 mmol, 0.04 mL) and phosphoric acid (0.05 mmol, 0.004 mL, 85%), and the solution stirred at room temperature overnight. The solvent was evaporated under a stream of air, and the crude reaction mixture was suspended in a small amount of EtOAc. Hexanes was added and the precipitate was collected by filtration and rinsed with hexanes and acetone. The precipitate was dried over vacuum to afford the desired product (74 mg, 68% yield) as a white powder. ^{1}H NMR (500 MHz, $CDCl_3$) δ 9.07 (s, 1H), 8.61 (s, 1H), 8.32 (d, *J* = 7.9 Hz,

1H), 7.61 (t, *J* = 6.6 Hz, 1H), 7.33 (d, J = 8.6 Hz, 2H), 7.08 (d, *J* = 8.7 Hz, 2H), 7.03 (d, *J* = 7.8 Hz, 1H), 5.57 (s, 1H), 4.16 (d, *J* = 17.9 Hz, 1H), 4.01 (d, *J* = 17.8 Hz, 1H), 1.98 – 1.67 (m, 2H), 1.68 – 1.49 (m, 4H), 1.45 – 1.28 (m, 1H), 1.27 (s, 9H), 1.24 – 0.64 (m, 3H). ^{13}C NMR (126 MHz, CDCl3) δ 166.94, 147.84, 143.94, 126.95, 125.47, 120.77, 115.57, 65.98, 48.79, 42.14, 34.47, 32.71, 32.32, 31.42, 31.21, 25.44, 24.68, 24.61.

***N*-(4-(*tert*-butyl)phenyl)-*N*-(2-(cyclohexylamino)-2-oxo-1-(pyridin-3-yl)ethyl)-3,3,3-trifluoro-2-oxopropanamide (6q).** To a solution of 4-tBu-aniline (0.62 mmol, 0.1 mL) in MeOH was added 3-Py-carboxaldehyde (0.62 mmol, 0.06 mL) and stirred for 30 min. The solution was cooled to 0ºC and trifluoropyruvic acid (0.62 mmol, 100 mg) and cyclohexyl isocyanide (0.62 mmol, 0.08 mL) were added. The solution was slowly warmed to r.t. and stirred overnight. The solvent was evaporated under a stream of air, and the crude reaction mixture was suspended in a small amount of EtOAc. Hexanes was added and the precipitate was collected by filtration and rinsed with hexanes and acetone. The precipitate was dried over vacuum to afford the desired product (87 mg, 29% yield) as a white powder. ^{1}H NMR (500 MHz, $CDCl_3$) δ 8.62 (s, 1H), 8.55 – 8.51 (m, 1H), 7.60 (d, J = 7.9 Hz, 1H), 7.23 (d, *J* = 8.6 Hz, 3H), 7.03 (s, 2H), 6.10 (s, 2H), 3.82 (tdt, *J* = 10.9, 7.8, 3.9 Hz, 1H), 1.90 (dd, J = 49.5, 12.9 Hz, 2H), 1.75 – 1.54 (m, 4H), 1.43 – 1.27 (m, 1H), 1.23 (s, 9H), 1.21 – 1.02 (m, 3H). ^{13}C NMR (126 MHz, CDCl3) δ 165.76, 162.63, 153.82, 150.12, 148.74, 139.63, 132.24, 130.28, 130.01, 126.64, 123.76, 62.36, 49.38, 34.89, 32.81, 32.79, 31.33, 31.21, 31.17, 25.49, 24.88, 24.83. ^{19}F NMR (471 MHz, $CDCl_3$) δ -74.82.

2-((cyanomethyl)amino)-*N*-cyclohexyl-2-(pyridin-3-yl)acetamide (7a). In a 6-dram vial equipped with a stir bar 3-Pyridinecarboxaldehyde (107 mg,1.0 mmol, 1.0 eq.) and b-alanine (89 mg, 1.0 mmol, 1.0 eq.) were mixed together in MeOH (4 mL).The obtained solution was stirred for 30 min. at room temperature. Cyclohexyl isocyanide (109 mg, 1.0 mmol, 1.0 eq.) was added to the reaction mixture and the walls of the vial were washed with 1 mL of MeOH. The obtained reaction mixture was stirred at room temperature overnight. The crude reaction mixture was evaporated in vacuo and redissolved in DCM. The obtained crude solution was deposited on silica. It was then purified using flash column chromatography using DCM/MeOH (gradient 0 → 5%) as eluent. The product was obtained as colorless oil, 156 mg 54%. ^{1}H NMR (500 MHz, $CDCl_3$) δ 8.65 (d, *J* = 2.4 Hz, 1H), 8.62 (dd, *J* = 4.8, 1.7 Hz, 1H), 7.75 (dt, *J* = 7.9, 2.0 Hz, 1H), 7.34 (dd, *J* = 7.9, 4.8 Hz, 1H), 6.02 (d, *J* = 8.4 Hz, 1H), 4.40 (s, 1H), 3.82 – 3.71 (m, 1H), 3.64 (d, *J* = 17.5 Hz, 1H), 3.45 (d, *J* = 17.3 Hz, 1H), 2.53 (s, 1H), 1.85 (ddd, *J* = 17.0, 12.4, 4.4 Hz, 2H), 1.64 (dtd, *J* = 25.9, 9.0, 4.7 Hz, 4H), 1.40 – 1.28 (m, 2H), 1.20 – 1.02 (m, 2H). ^{13}C NMR (126 MHz, $CDCl_3$) δ 168.45, 150.57, 149.43, 135.66, 133.25, 124.24, 116.87, 63.55, 48.67, 35.50, 33.06, 33.02,

25.49, 24.83. HRMS (ESI/Q-TOF) m/z: $[M + Na]^+$ calculated for $C_{15}H_{20}N_4NaO$ 295.1529 ; found 295.1523.

***N*-cyclohexyl-2-(2-oxoazetidin-1-yl)-2-(pyridin-3-yl)acetamide (7b).** In a 6-dram vial equipped with a stir bar 3-Pyridinecarboxaldehyde (214 mg, 2.0 mmol, 1.0 eq.), glycinamide hydrochloride (221 mg, 2.0 mmol, 1.0 eq.), and triethylamine (202 mg, 2.0 mmol, 1.0 eq.), were mixed together in methanol (5 mL). The obtained solution was stirred for 15 min at room temperature. Afterwards cyclohexyl isocyanide (218 mg, 2.0 mmol, 1.0 eq.), and acetic acid (120 mg, 2.0 mmol, 1.0 eq.) was added to the reaction mixture and the walls of the vial were washed with additional MeOH (5 mL). The reaction mixture was stirred at room temperature overnight. The crude reaction mixture was evaporated in vacuo and redissolved in EtOAc (50 mL). The organic layer was extracted with water (3 x 100 mL). The obtained organic layer was dried over Na_2SO_4 and evaporated in vacuo. The obtained crude solid was triturated with hexanes (5 mL) and filtered. The Obtained powder was further washed Hexanes (2 x 5 mL). The product was obtained as pale-yellow solid, 428 mg 79%. ^{1}H NMR (500 MHz, $CDCl_3$) δ 8.59 (s, 2H), 7.75 (dd, *J* = 8.0, 2.1 Hz, 1H), 7.32 (dd, *J* = 8.0, 4.9 Hz, 1H), 6.40 (d, *J* = 7.9 Hz, 1H), 5.34 (s, 0H), 3.76 (dtt, *J* = 11.4, 8.5, 4.0 Hz, 1H), 3.61 (td, *J* = 5.6, 2.8 Hz, 1H), 3.20 (td, *J* = 5.7, 2.8 Hz, 1H), 3.05 – 2.97 (m, 1H), 2.95 – 2.87 (m, 1H), 1.94 – 1.83 (m, 2H), 1.73 – 1.55 (m, 2H), 1.43 – 1.26 (m, 3H), 1.22 – 0.98 (m, 4H). ^{13}C NMR (126 MHz, $CDCl_3$) δ 168.10, 166.82, 150.04, 149.62, 135.82, 130.98, 123.90, 58.10, 48.97, 39.28, 36.53, 32.89, 32.85, 29.84, 25.52, 24.82, 24.78.

(*E*)-*N*-(4-(*tert*-butyl)phenyl)-*N*-(2-(*tert*-butylamino)-2-oxo-1-(pyridin-3-yl)ethyl)but-2-enamide (8a). Compound was purified using general procedure A, white solid 54 % yield, 198 mg. ^{1}H NMR (500 MHz, $CDCl_3$) δ 8.48 – 8.41 (m, 2H), 7.43 (d, J = 8.0 Hz, 1H), 7.26 (d, J = 8.2 Hz, 2H), 7.05 (dd, J = 8.0, 4.8 Hz, 1H), 7.01 – 6.95 (m, 1H), 6.91 (s, 1H), 6.35 (s, 1H), 6.07 (s, 1H), 5.68 (dd, J = 15.1, 1.7 Hz, 1H), 1.75 (dd, J = 7.1, 1.7 Hz, 3H), 1.39 (s, 9H), 1.30 (s, 9H).^{13}C NMR (126 MHz, $CDCl_3$) δ 168.38, 166.89, 151.78, 151.38, 149.47, 142.97, 138.10, 136.53, 130.94, 129.85, 126.20, 122.77, 63.16, 51.73, 34.76, 31.38, 28.81, 18.21. HRMS (ESI/Q-TOF) m/z: $[M + Na]^+$ calculated for $C_{25}H_{33}N_3NaO_2$ 430.2438; found 430.2450.

***N*-(4-(*tert*-butyl)phenyl)-*N*-(2-(*tert*-butylamino)-2-oxo-1-(pyridin-3-yl)ethyl)but-2-ynamide (8b).** Compound was purified using general procedure A, white solid 82 % yield, 300 mg. ^{1}H NMR (500 MHz, $CDCl_3$) δ 8.45 (dd, J = 4.8, 1.5 Hz, 1H), 8.43 (d, J = 2.3 Hz, 1H), 7.43 (dt, J = 8.1, 2.0 Hz, 1H), 7.25 – 7.20 (m, 2H), 7.05 (dd, J = 8.0, 4.8 Hz, 1H), 6.97 (d, J = 8.0 Hz, 2H), 6.09 (s, 1H), 5.96 (s, 1H), 1.68 (s,

3H), 1.36 (s, 9H), 1.26 (s, 9H). ^{13}C NMR (126 MHz, $CDCl_3$) δ 167.54, 155.43, 151.94, 151.27, 149.67, 138.25, 136.37, 130.29, 129.91, 125.77, 122.95, 92.21, 73.90, 62.66, 51.98, 34.76, 31.35, 28.75. HRMS (ESI/Q-TOF) m/z: $[M + Na]^+$ calculated for $C_{25}H_{31}N_3NaO_2$ 428.2308; found 428.2307.

***N*-(4-(*tert*-butyl)phenyl)-*N*-(2-(*tert*-butylamino)-2-oxo-1-(pyridin-3-yl)ethyl)acrylamide (8c).** Compound was purified using general procedure C, white solid 42 % yield, 150 mg. ^{1}H NMR (500 MHz, $CDCl_3$) δ 8.46 – 8.42 (m, 2H), 7.43 (dt, *J* = 8.0, 2.0 Hz, 1H), 7.24 (d, *J* = 8.3 Hz, 2H), 7.04 (ddd, *J* = 8.0, 4.9, 0.9 Hz, 1H), 6.91 (s, 1H), 6.40 (dd, *J* = 16.8, 2.0 Hz, 1H), 6.20 (s, 1H), 6.06 (s, 1H), 5.98 (dd, *J* = 16.8, 10.3 Hz, 1H), 5.55 (dd, *J* = 10.3, 2.0 Hz, 1H), 1.37 (s, 9H), 1.26 (s, 9H). ^{13}C NMR (126 MHz, $CDCl_3$) δ 168.13, 166.58, 152.00, 151.38, 149.58, 138.15, 136.19, 130.77, 129.89, 128.77, 128.60, 126.25, 122.87, 63.18, 51.84, 34.77, 31.37, 28.80. HRMS (ESI/Q-TOF) m/z: $[M + Na]^+$ calculated for $C_{24}H_{31}N_3NaO_2$ 416.2308; found 416.2291.

***N*-(*tert*-butyl)-2-(*N*-(4-(*tert*-butyl)phenyl)acetamido)-2-(pyridin-3-yl)acetamide (8d).** Compound was purified using general procedure A, white solid 84 % yield, 290 mg. ^{1}H NMR (500 MHz, $CDCl_3$) δ 8.43 (dd, *J* = 4.8, 1.6 Hz, 1H), 8.40 (s, 1H), 7.37 (d, *J* = 8.1 Hz, 1H), 7.22 (d, *J* = 8.2 Hz, 2H), 7.01 (dd, *J* = 7.6, 5.3 Hz, 1H), 6.91 (s, 1H), 6.04 (s, 1H), 5.98 (s, 1H), 1.87 (s, 3H), 1.36 (s, 9H), 1.25 (s, 9H). ^{13}C NMR (126 MHz, $CDCl_3$) δ 171.75, 168.32, 151.86, 151.45, 149.59, 138.13, 137.31, 130.88, 129.65, 126.24, 122.84, 62.64, 51.80, 34.72, 31.36, 28.79, 23.36. HRMS (ESI/Q-TOF) m/z: $[M + Na]^+$ calculated for $C_{23}H_{31}N_3NaO_2$ 404.2308; found 404.2307.

***N*-(4-(tert-butyl)phenyl)-*N*-(2-(cyclopentylamino)-2-oxo-1-(pyridin-3-yl)ethyl)but-2-ynamide (8e).** Compound was purified using general procedure A, white solid 94 % yield, 354 mg. ^{1}H NMR (500 MHz, $CDCl_3$) δ 8.46 (dd, *J* = 4.9, 1.6 Hz, 1H), 8.44 (d, *J* = 2.3 Hz, 1H), 7.50 – 7.44 (m, 1H), 7.23 (d, *J* = 8.8 Hz, 2H), 7.07 (dd, *J* = 8.0, 4.8 Hz, 1H), 6.97 (d, *J* = 8.0 Hz, 2H), 6.20 (s, 1H), 6.02 (s, 1H), 4.23 (h, *J* = 6.8 Hz, 1H), 2.02 (dd, *J* = 13.0, 6.2 Hz, 1H), 1.95 (q, *J* = 2.7 Hz, 1H), 1.68 (s, 3H), 1.64 – 1.56 (m, 4H), 1.49 – 1.42 (m, 1H), 1.39 – 1.34 (m, 1H), 1.26 (s, 9H). ^{13}C NMR (126 MHz, $CDCl_3$) δ 167.92, 155.47, 151.97, 151.06, 149.54, 138.34, 136.39, 130.32, 129.87, 125.79, 123.06, 92.26, 73.85, 62.23, 51.89, 34.76, 33.08, 33.01, 31.34, 23.87, 23.84, 4.06.

***N*-(2-(benzylamino)-2-oxo-1-(pyridin-3-yl)ethyl)-*N*-(4-(*tert*-butyl)phenyl)but-2-ynamide (8f).** Compound was purified using general procedure A, pale yellow solid 86 % yield, 340 mg. ^{1}H NMR (500 MHz, $CDCl_3$) δ 8.43 (d, *J* = 4.7 Hz, 1H), 8.40 (t, *J* = 1.6 Hz, 2H), 7.45 (d, *J* = 7.8 Hz, 1H), 7.33 – 7.16 (m, 6H), 7.05 (dd, *J* = 8.0, 4.8 Hz, 1H), 6.94 (d, *J* = 8.1 Hz, 2H), 6.66 (d, *J* = 8.5 Hz, 1H), 6.05 (s, 1H),

4.55 – 4.43 (m, 2H), 1.66 (s, 3H), 1.25 (s, 9H). ^{13}C NMR (126 MHz, $CDCl_3$) δ 168.38, 155.47, 151.96, 151.08, 149.59, 138.41, 137.91, 136.33, 130.18, 129.93, 128.85, 127.84, 127.64, 125.78, 123.11, 92.27, 73.83, 62.35, 44.02, 34.74, 31.65, 31.33, 4.04.

***N*-(4-(*tert*-butyl)phenyl)-2-chloro-*N*-(2-(cyclopentylamino)-2-oxo-1-(pyridin-3-yl)ethyl)acetamide (8g).** Compound was purified using general procedure A, pale yellow solid 88 % yield, 340 mg. ^{1}H NMR (500 MHz, $CDCl_3$) δ 8.46 (dd, *J* = 4.9, 1.7 Hz, 1H), 8.42 (d, *J* = 2.3 Hz, 1H), 7.44 (dd, *J* = 8.0, 2.1 Hz, 1H), 7.26 (s, 3H), 7.06 (dd, *J* = 8.0, 4.8 Hz, 1H), 6.06 (d, *J* = 7.3 Hz, 1H), 5.99 (s, 1H), 4.23 (h, *J* = 6.8 Hz, 1H), 3.85 (s, 2H), 2.10 – 1.99 (m, 1H), 1.98 – 1.90 (m, 1H), 1.70 – 1.52 (m, 4H), 1.51 – 1.40 (m, 1H), 1.33 (dq, *J* = 13.6, 6.8, 5.8 Hz, 1H), 1.25 (s, 9H). ^{13}C NMR (126 MHz, $CDCl_3$) δ 167.93, 167.42, 152.82, 151.20, 149.68, 138.30, 135.29, 130.25, 129.75, 126.59, 123.16, 63.03, 51.94, 42.61, 34.83, 33.08, 33.03, 31.32, 23.88, 23.86.

***N*-benzyl-2-(*N*-(4-(*tert*-butyl)phenyl)-2-chloroacetamido)-2-(pyridin-3-yl)acetamide (8h).** Compound was purified using general procedure A, yellow solid 91 % yield, 370 mg. ^{1}H NMR (500 MHz, $CDCl_3$) δ 8.45 (dd, *J* = 4.8, 1.6 Hz, 1H), 8.40 (d, *J* = 2.3 Hz, 1H), 7.43 (dt, *J* = 8.0, 2.1 Hz, 1H), 7.35 – 7.13 (m, 9H), 7.04 (ddd, *J* = 8.1, 4.9, 0.9 Hz, 1H), 6.55 (s, 1H), 6.06 (s, 1H), 4.49 (qd, *J* = 14.8, 5.8 Hz, 2H), 3.85 (d, *J* = 1.5 Hz, 2H), 1.25 (s, 9H). ^{13}C NMR (126 MHz, $CDCl_3$) δ 168.45, 167.46, 152.84, 151.36, 149.93, 138.24, 137.84, 135.18, 129.95, 129.79, 128.86, 127.83, 127.70, 126.59, 123.14, 63.10, 44.07, 42.67, 34.82, 31.31.

***N*-(4-(tert-butyl)phenyl)-*N*-(2-(cyclopentylamino)-2-oxo-1-(pyridin-3-yl)ethyl)cyclopent-1-ene-1-carboxamide (8i).** Compound was purified using general procedure B, off white solid 67 % yield, 270 mg. ^{1}H NMR (500 MHz, $CDCl_3$) δ 8.51 (d, *J* = 2.3 Hz, 1H), 8.49 (dd, *J* = 4.8, 1.7 Hz, 1H), 7.54 (dt, *J* = 8.0, 2.0 Hz, 1H), 7.25 – 7.19 (m, 2H), 7.11 (ddd, *J* = 8.0, 4.8, 0.8 Hz, 1H), 6.92 (d, *J* = 8.0 Hz, 2H), 6.35 (d, *J* = 7.4 Hz, 1H), 6.05 (s, 1H), 5.85 (p, *J* = 2.2 Hz, 1H), 4.28 (q, *J* = 6.7 Hz, 1H), 2.22 (ddd, *J* = 7.6, 6.1, 2.5 Hz, 2H), 2.15 (tt, *J* = 6.4, 2.2 Hz, 2H), 2.10 – 1.93 (m, 2H), 1.65 – 1.64 (m, 6H), 1.53 – 1.35 (m, 2H), 1.28 (s, 9H). ^{13}C NMR (126 MHz, $CDCl_3$) δ 168.81, 168.55, 151.49, 151.12, 149.40, 140.09, 138.96, 137.84, 137.57, 130.79, 129.37, 125.73, 122.83, 63.78, 51.62, 34.60, 33.71, 33.13, 33.01, 32.97, 31.25, 23.73, 23.71, 23.18.

***N*-(4-(*tert*-butyl)phenyl)-*N*-(2-(cyclohexylamino)-2-oxo-1-(thiophen-3-yl)ethyl)cyclopent-1-ene-1-carboxamide (9a).** Compound was purified using general procedure B, off white solid 79 % yield, 330 mg. ^{1}H NMR (500 MHz, $CDCl_3$) δ 7.27 – 7.24 (m, 1H), 7.20 – 7.12 (m, 3H), 6.94 – 6.87 (m, 3H), 6.09

(d, *J* = 8.1 Hz, 1H), 6.06 (s, 1H), 5.81 (q, *J* = 2.2 Hz, 1H), 3.87 – 3.76 (m, 1H), 2.22 – 2.06 (m, 4H), 2.01 – 1.84 (m, 2H), 1.71 – 1.53 (m, 5H), 1.42 – 1.28 (m, 2H), 1.26 (s, 9H), 1.15 (ddt, *J* = 16.1, 12.0, 8.0 Hz, 3H). ^{13}C NMR (126 MHz, $CDCl_3$) δ 168.73, 168.53, 151.12, 139.46, 139.40, 138.34, 135.52, 129.16, 129.08, 126.40, 125.51, 125.33, 61.62, 48.59, 34.68, 33.83, 33.19, 32.97, 32.93, 31.42, 25.67, 24.88, 24.83, 23.36. HRMS (ESI/Q-TOF) m/z: $[M + Na]^+$ calculated for $C_{28}H_{36}N_2NaO_2S$ 487.2390; found 487.2404.

***N*-(4-(*tert*-butyl)phenyl)-*N*-(2-(cyclohexylamino)-2-oxo-1-(quinolin-3-yl)ethyl)cyclopent-1-ene-1-carboxamide (9b).** Compound was purified using general procedure B, pale yellow solid 59 % yield, 270 mg. H NMR (500 MHz, $CDCl_3$) δ 8.73 (d, *J* = 2.1 Hz, 1H), 8.03 (d, *J* = 8.4 Hz, 1H), 8.00 (s, 1H), 7.74 – 7.66 (m, 1H), 7.65 – 7.61 (m, 1H), 7.52 – 7.45 (m, 1H), 7.13 (d, *J* = 8.2 Hz, 2H), 6.39 (s, 2H), 6.27 (s, 1H), 5.86 (p, *J* = 2.3 Hz, 1H), 3.93 – 3.82 (m, 1H), 2.23 – 2.09 (m, 4H), 2.00 (dd, *J* = 12.2, 4.1 Hz, 2H), 1.89 (dd, *J* = 12.8, 4.2 Hz, 1H), 1.66 (p, *J* = 7.7 Hz, 5H), 1.36 (ddd, *J* = 16.2, 13.1, 11.4 Hz, 2H), 1.19 (s, 9H), 1.18 – 1.08 (m, 3H). ^{13}C NMR (126 MHz, $CDCl_3$) δ 169.02, 168.29, 151.91, 151.58, 147.65, 140.28, 139.13, 138.06, 137.59, 130.00, 129.59, 129.15, 128.23, 127.98, 127.47, 126.87, 125.83, 63.71, 48.83, 34.69, 33.87, 33.26, 33.02, 32.98, 31.31, 25.62, 24.90, 24.85, 23.32. HRMS (ESI/Q-TOF) m/z: $[M + Na]^+$ calculated for $C_{33}H_{39}N_3NaO_2$ 532.2934; found 532.2946.

***N*-(1-(benzo[b]thiophen-3-yl)-2-(cyclohexylamino)-2-oxoethyl)-*N*-(4-(*tert*-butyl)phenyl)cyclopent-1-ene-1-carboxamide (9c).** Compound was purified using general procedure B, pale yellow solid 26 % yield, 120 mg. ^{1}H NMR (500 MHz, $CDCl_3$) δ 7.83 (d, *J* = 7.6 Hz, 1H), 7.78 – 7.72 (m, 1H), 7.53 (s, 1H), 7.37 (p, *J* = 7.0 Hz, 2H), 7.03 (d, *J* = 8.2 Hz, 2H), 6.69 (d, *J* = 19.7 Hz, 3H), 6.20 (d, *J* = 8.2 Hz, 1H), 5.84 – 5.79 (m, 1H), 2.17 – 2.00 (m, 4H), 1.97 – 1.90 (m, 2H), 1.65 (pt, *J* = 14.3, 6.5 Hz, 5H), 1.36 (ddt, *J* = 15.3, 11.9, 6.0 Hz, 3H), 1.19 (s, 12H). ^{13}C NMR (126 MHz, $CDCl_3$) δ 169.16, 168.29, 151.15, 139.68, 139.60, 139.30, 138.74, 137.04, 129.40, 129.26, 129.10, 125.16, 124.61, 124.59, 122.92, 121.61, 57.25, 48.65, 34.61, 33.87, 33.18, 33.04, 32.98, 31.36, 25.65, 24.94, 24.89, 23.36. HRMS (ESI/Q-TOF) m/z: $[M + Na]^+$ calculated for $C_{32}H_{38}N_2NaO_2S$ 537.2546; found 537.2549.

***N*-(4-(*tert*-butyl)phenyl)-*N*-(2-(cyclohexylamino)-2-oxo-1-(pyridin-4-yl)ethyl)cyclopent-1-ene-1-carboxamide (9d).** Compound was purified using general procedure B, white solid 371 % yield, 90 mg. ^{1}H NMR (500 MHz, $CDCl_3$) δ 8.49 (d, *J* = 6.2 Hz, 2H), 7.30 – 7.19 (m, 4H), 6.97 (d, *J* = 8.1 Hz, 2H), 6.45 (d, *J* = 8.1 Hz, 1H), 5.88 (p, *J* = 2.2 Hz, 1H), 5.82 (s, 1H), 3.89 – 3.78 (m, 1H), 2.21 (ddt, *J* = 7.6, 5.0, 2.6 Hz, 2H), 2.12 (dtt, *J* = 9.9, 5.0, 2.2 Hz, 2H), 1.98 – 1.84 (m, 3H), 1.67 (p, *J* = 7.4 Hz, 4H), 1.43 –

1.29 (m, 2H), 1.26 (s, 9H), 1.19 (dddd, *J* = 26.8, 22.7, 10.8, 4.5 Hz, 3H). ^{13}C NMR (126 MHz, $CDCl_3$) δ 169.03, 167.76, 151.65, 149.80, 144.29, 140.77, 139.08, 138.60, 128.71, 126.05, 124.23, 67.01, 48.74, 34.76, 33.69, 33.27, 32.92, 32.88, 31.39, 25.62, 24.80, 23.34.

***N*-(4-(*tert*-butyl)phenyl)-*N*-(2-(cyclohexylamino)-2-oxo-1-(pyrimidin-5-yl)ethyl)cyclopent-1-ene-1-carboxamide (9e).** Compound was purified using general procedure B, off white solid 29 % yield, 120 mg. ^{1}H NMR (500 MHz, $CDCl_3$) δ 9.06 (s, 1H), 8.55 (s, 2H), 7.25 (d, *J* = 8.9 Hz, 2H), 6.85 (dd, *J* = 15.8, 5.0 Hz, 2H), 6.62 (d, *J* = 8.1 Hz, 1H), 6.18 (s, 1H), 5.84 (td, *J* = 2.7, 1.3 Hz, 1H), 3.89 – 3.78 (m, 1H), 2.55 (dd, *J* = 25.2, 2.4 Hz, 2H), 2.20 (ddd, *J* = 7.8, 6.0, 2.5 Hz, 2H), 2.12 (ddd, *J* = 10.3, 5.6, 2.3 Hz, 2H), 2.01 – 1.86 (m, 1H), 1.76 – 1.57 (m, 5H), 1.46 – 1.31 (m, 2H), 1.27 (s, 9H), 1.26 – 1.14 (m, 3H). ^{13}C NMR (101 MHz, $CDCl_3$) δ 169.14, 167.31, 158.59, 158.11, 152.37, 145.94, 141.02, 138.68, 136.78, 129.38, 128.84, 126.31, 61.37, 48.85, 34.82, 33.84, 33.70, 33.32, 32.99, 32.91, 31.36, 31.32, 25.60, 24.79, 23.31, 23.29. HRMS (ESI/Q-TOF) m/z: $[M + Na]^+$ calculated for $C_{28}H_{36}N_4NaO_2$ 483.2730; found 483.2746.

***N*-(4-(*tert*-butyl)phenyl)-*N*-(2-(cyclohexylamino)-1-(isoquinolin-4-yl)-2-oxoethyl)cyclopent-1-ene-1-carboxamide (9f).** Compound was purified using general procedure A, off white solid 78 % yield, 358 mg. ^{1}H NMR (500 MHz, $CDCl_3$) δ 9.08 (d, *J* = 1.9 Hz, 1H), 8.28 (s, 1H), 8.01 (d, *J* = 8.5 Hz, 1H), 7.95 (d, *J* = 8.1 Hz, 1H), 7.77 (dd, *J* = 8.5, 6.9 Hz, 1H), 7.66 – 7.59 (m, 1H), 7.06 (s, 1H), 6.93 (d, *J* = 8.1 Hz, 2H), 6.78 (s, 1H), 5.81 (q, *J* = 2.1 Hz, 1H), 5.67 (s, 1H), 3.91 (dt, *J* = 7.5, 3.5 Hz, 1H), 2.21 – 2.09 (m, 4H), 1.97 (d, *J* = 16.2 Hz, 2H), 1.72 – 1.62 (m, 5H), 1.34 (tdd, *J* = 12.3, 8.3, 3.8 Hz, 2H), 1.13 (d, *J* = 0.9 Hz, 12H). ^{13}C NMR (126 MHz, $CDCl_3$) δ 168.96, 168.39, 153.31, 151.05, 145.51, 139.71, 139.19, 136.80, 135.07, 131.47, 129.61, 128.57, 128.14, 127.44, 125.06, 124.84, 122.71, 58.84, 49.11, 34.52, 33.87, 33.23, 33.04, 33.00, 31.28, 25.61, 25.00, 24.89, 23.34. HRMS (ESI/Q-TOF) m/z: $[M + Na]^+$ calculated for $C_{33}H_{39}N_3NaO_2$ 532.2934; found 532.2932.

***N*-(4-(*tert*-butyl)phenyl)-*N*-(2-(cyclohexylamino)-1-(1*H*-imidazol-5-yl)-2-oxoethyl)cyclopent-1-ene-1-carboxamide (9g).** Compound was purified using general procedure B, off white solid 37 % yield, 150 mg. ^{1}H NMR (500 MHz, $CDCl_3$) δ 7.61 (d, *J* = 1.0 Hz, 1H), 7.28 (d, *J* = 8.6 Hz, 2H), 7.11 (s, 1H), 7.00 (d, *J* = 8.2 Hz, 2H), 6.81 (d, *J* = 2.5 Hz, 1H), 5.86 (p, *J* = 2.3 Hz, 1H), 5.75 (s, 1H), 3.79 (td, *J* = 6.3, 3.4 Hz, 1H), 2.60 (ddd, *J* = 10.0, 4.9, 2.3 Hz, 2H), 2.52 (ddt, *J* = 7.7, 5.2, 2.6 Hz, 2H), 2.21 (ddt, *J* = 7.6, 5.0, 2.5 Hz, 2H), 1.85 (d, *J* = 14.6 Hz, 2H), 1.73 – 1.65 (m, 4H), 1.37 – 1.22 (m, 15H). ^{13}C NMR (101 MHz, $CDCl_3$) δ 169.46, 167.62, 158.91, 158.43, 152.68, 146.26, 141.34, 139.00, 137.10, 129.70, 129.15, 126.63, 61.69, 49.16, 35.14, 34.15, 34.02, 33.64, 33.31, 33.22, 31.67, 31.64, 25.92, 25.11, 23.63, 23.60.

(*E*)-*N*-(4-(*tert*-butyl)phenyl)-*N*-(2-(cyclohexylamino)-2-oxo-1-(pyridin-4-yl)ethyl)but-2-enamide (9h). Compound was purified using general procedure A, white solid 74 % yield, 287 mg. ^{1}H NMR (500 MHz, $CDCl_3$) δ 8.49 – 8.45 (m, 2H), 7.28 (d, *J* = 8.9 Hz, 2H), 7.19 – 7.12 (m, 2H), 7.03 – 6.92 (m, 3H), 6.47 (d, *J* = 7.9 Hz, 1H), 5.84 (s, 1H), 5.70 (dd, *J* = 15.0, 1.8 Hz, 1H), 4.03 – 3.75 (m, 1H), 1.95 (dd, *J* = 12.3, 4.3 Hz, 1H), 1.91 – 1.85 (m, 1H), 1.78 – 1.74 (m, 3H), 1.70 – 1.64 (m, 2H), 1.58 (dt, *J* = 12.9, 3.9 Hz, 1H), 1.37 – 1.31 (m, 2H), 1.29 (s, 9H), 1.25 – 1.08 (m, 3H). ^{13}C NMR (126 MHz, $CDCl_3$) δ 167.84, 167.10, 151.87, 149.73, 144.20, 143.48, 137.54, 129.06, 126.42, 124.35, 122.64, 66.12, 48.75, 34.80, 32.89, 31.39, 25.62, 24.83, 24.80, 18.25. HRMS (ESI/Q-TOF) m/z: $[M + Na]^+$ calculated for $C_{27}H_{35}N_3NaO_2$ 456.2621; found 456.2614.

***N*-(4-(*tert*-butyl)phenyl)-2-chloro-*N*-(2-(cyclohexylamino)-2-oxo-1-(thiophen-3-yl)ethyl)acetamide (9i).** Compound was purified using general procedure A, white solid 87 % yield, 352 mg. ^{1}H NMR (500 MHz, $CDCl_3$) δ 7.28 (s, 2H), 7.25 – 7.21 (m, 1H), 7.17 (dd, *J* = 5.0, 3.0 Hz, 1H), 6.84 (dd, *J* = 5.0, 1.3 Hz, 1H), 6.01 (s, 1H), 5.79 (d, *J* = 8.2 Hz, 1H), 3.87 (s, 2H), 3.82 (ddt, *J* = 14.7, 6.7, 3.9 Hz, 1H), 1.98 – 1.92 (m, 1H), 1.91 – 1.85 (m, 1H), 1.74 – 1.60 (m, 3H), 1.38 (dqd, *J* = 8.3, 3.3, 1.6 Hz, 2H), 1.30 (s, 9H), 1.23 – 1.05 (m, 3H). ^{13}C NMR (126 MHz, $CDCl_3$) δ 167.83, 166.99, 152.39, 136.30, 134.59, 129.25, 128.85, 126.93, 126.34, 125.82, 61.28, 48.89, 42.69, 34.81, 32.95 (d, *J* = 10.4 Hz),31.57, 31.38, 25.62, 24.90, 24.84.

***N*-(4-(*tert*-butyl)phenyl)-2-chloro-*N*-(2-(cyclohexylamino)-2-oxo-1-(pyridin-4-yl)ethyl)acetamide (9j).** Compound was purified using general procedure A, white solid 94 % yield, 375 mg. ^{1}H NMR (500 MHz, $CDCl_3$) δ 8.47 (d, *J* = 6.1 Hz, 2H), 7.26 (s, 2H), 7.16 – 7.11 (m, 2H), 5.88 (d, *J* = 8.0 Hz, 1H), 5.83 (s, 1H), 3.87 (d, *J* = 1.9 Hz, 2H), 3.85 – 3.77 (m, 1H), 2.00 – 1.94 (m, 1H), 1.86 (dd, *J* = 12.9, 4.0 Hz, 1H), 1.75 – 1.53 (m, 3H), 1.41 – 1.28 (m, 2H), 1.26 (s, 9H), 1.23 – 1.03 (m, 3H). ^{13}C NMR (126 MHz, $CDCl_3$) δ 167.57, 166.93, 152.92, 149.88, 143.19, 135.93, 129.26, 126.68, 124.90, 65.47, 49.11, 42.49, 34.87, 32.90, 32.85, 31.33, 25.56, 24.88, 24.82.

***N*-(4-(*tert*-butyl)phenyl)-2-chloro-*N*-(2-(cyclohexylamino)-1-(5-methylpyrazin-2-yl)-2-oxoethyl)acetamide (9k).** Compound was purified using general procedure B, pale yellow solid 34 % yield, 140 mg. ^{1}H NMR (500 MHz, $CDCl_3$) δ 8.62 (s, 1H), 8.39 (s, 1H), 7.37 (d, *J* = 8.2 Hz, 2H), 7.29 – 7.06 (m, 2H), 5.88 (s, 1H), 3.89 (q, *J* = 13.6 Hz, 2H), 3.82 – 3.72 (m, 1H), 1.92 – 1.85 (m, 3H), 1.77 – 1.53 (m, 5H), 1.32 (s, 13H), 1.22 – 1.12 (m, 2H). ^{13}C NMR (126 MHz, $CDCl_3$) δ 167.11, 165.73, 153.11,

152.59, 147.62, 144.81, 142.87, 136.87, 128.87, 126.66, 65.99, 48.50, 42.31, 34.75, 32.59, 32.49, 31.60, 31.24, 25.48, 24.57, 24.50, 22.66, 21.31, 14.13.

***N*-(4-(*tert*-butyl)phenyl)-N-(2-(cyclohexylamino)-1-(isoquinolin-4-yl)-2-oxoethyl)but-2-ynamide (9l).** Compound was purified using general procedure A, pale white solid 90 % yield, 392 mg. ^{1}H NMR (500 MHz, $CDCl_3$) δ 9.11 (d, *J* = 0.7 Hz, 1H), 8.24 (s, 1H), 8.00 – 7.94 (m, 2H), 7.82 – 7.73 (m, 1H), 7.65 (ddd, *J* = 7.9, 6.9, 1.0 Hz, 1H), 7.00 (d, *J* = 8.1 Hz, 2H), 6.95 (s, 1H), 6.86 (s, 2H), 5.62 (d, *J* = 8.1 Hz, 1H), 3.89 (dtd, *J* = 10.8, 7.8, 7.2, 3.9 Hz, 1H), 2.01 – 1.94 (m, 1H), 1.93 (s, 1H), 1.65 (s, 6H), 1.31 (d, *J* = 18.7 Hz, 2H), 1.15 (s, 9H), 1.10 – 0.97 (m, 3H). ^{13}C NMR (126 MHz, CDCl3) δ 167.30, 155.31, 153.07, 151.22, 144.79, 135.59, 134.71, 131.56, 129.62, 128.48, 127.90, 127.41, 124.89, 124.21, 122.31, 91.66, 73.65, 57.76, 48.95, 34.33, 32.74, 32.68, 30.99, 25.32, 24.73, 24.63, 3.79, 3.63.

***N*-(4-(*tert*-butyl)phenyl)-N-(2-(cyclohexylamino)-2-oxo-1-(quinolin-3-yl)ethyl)but-2-ynamide (9m).** Compound was purified using general procedure A, pale white solid 69 % yield, 298 mg. ^{1}H NMR (500 MHz, $CDCl_3$) δ 8.70 (d, *J* = 2.2 Hz, 1H), 8.07 (dd, *J* = 8.4, 1.0 Hz, 1H), 8.00 (d, *J* = 2.4 Hz, 1H), 7.73 – 7.70 (m, 1H), 7.65 (dd, *J* = 8.2, 1.4 Hz, 1H), 7.52 (ddd, *J* = 8.1, 6.8, 1.2 Hz, 1H), 7.21 (d, *J* = 8.8 Hz, 2H), 7.01 (d, *J* = 8.0 Hz, 2H), 6.27 (s, 1H), 6.23 – 6.18 (m, 1H), 3.95 – 3.83 (m, 1H), 2.05 – 1.99 (m, 1H), 1.92 – 1.84 (m, 1H), 1.78 – 1.58 (m, 6H), 1.47 – 1.35 (m, 3H), 1.23 (s, 9H), 1.21 – 1.10 (m, 3H). ^{13}C NMR (126 MHz, CDCl3) δ 167.79, 155.80, 152.21, 151.92, 147.77, 138.75, 136.61, 130.53, 130.17, 129.23, 128.49, 127.69, 127.51, 127.29, 126.06, 92.59, 74.16, 49.31, 35.00, 33.22, 33.15, 31.54, 25.85, 25.15, 25.11, 23.05, 14.51, 4.35.

***N*-(1-(benzo[d]thiazol-2-yl)-2-(cyclohexylamino)-2-oxoethyl)-*N*-(4-(*tert*-butyl)phenyl)but-2-ynamide (9n).** Compound was purified using general procedure A, pale white solid 91 % yield, 398 mg. ^{1}H NMR (500 MHz, $CDCl_3$) δ 9.61 (d, *J* = 7.9 Hz, 1H), 8.11 – 8.00 (m, 1H), 7.95 – 7.84 (m, 1H), 7.56 – 7.51 (m, 1H), 7.47 (d, *J* = 1.2 Hz, 1H), 7.46 – 7.35 (m, 2H), 7.29 – 7.22 (m, 2H), 6.15 (d, *J* = 1.6 Hz, 1H), 4.04 – 3.94 (m, 1H), 1.99 (d, *J* = 1.6 Hz, 3H), 1.91 – 1.64 (m, 4H), 1.55 – 1.34 (m, 6H), 1.24 (s, 9H). ^{13}C NMR (126 MHz, $CDCl_3$) δ 171.84, 169.60, 163.31, 158.61, 152.14, 148.14, 135.47, 134.80, 126.83, 126.70, 126.56, 126.18, 124.24, 123.56, 122.32, 121.64, 121.47, 50.84, 49.26, 34.67, 32.77, 32.67, 31.72, 31.59, 31.37, 25.94, 25.14, 24.84, 24.68, 24.60, 13.39, 4.08.

***N*-(1-(benzo[b]thiophen-3-yl)-2-(cyclohexylamino)-2-oxoethyl)-*N*-(4-(*tert*-butyl)phenyl)but-2-ynamide (9o).** Compound was purified using general procedure A, grey solid 92 % yield, 402 mg. ^{1}H NMR (500 MHz, $CDCl_3$) δ 7.86 – 7.82 (m, 1H), 7.77 – 7.71 (m, 1H), 7.50 (s, 1H), 7.45 – 7.34 (m, 2H),

7.14 – 7.08 (m, 2H), 6.82 (s, 2H), 6.65 (s, 1H), 6.04 (d, *J* = 8.2 Hz, 1H), 3.88 (dddd, *J* = 14.5, 10.5, 7.9, 3.9 Hz, 1H), 2.01 – 1.91 (m, 1H), 1.92 – 1.87 (m, 1H), 1.79 – 1.60 (m, 6H), 1.47 – 1.28 (m, 3H), 1.23 (s, 9H), 1.21 – 1.07 (m, 2H). ^{13}C NMR (126 MHz, $CDCl_3$) δ 167.45, 155.48, 151.34, 139.47, 138.29, 136.01, 129.42, 129.35, 128.26, 125.05, 124.60, 124.58, 122.81, 121.41, 91.83, 73.83, 56.30, 48.74, 34.53, 32.83, 32.79, 31.19, 25.49, 24.79, 24.75, 3.93.

***N*-(2-(cyclohexylamino)-2-oxo-1-(pyridin-3-yl)ethyl)-2-oxo-*N*-(*m*-tolyl)propanamide (10a).** Compound was prepared according to the procedure for 13. Pale yellow solid, 134 mg, 37% yield. ^{1}H NMR (500 MHz, $CDCl_3$) δ 8.63 (d, *J* = 5.7 Hz, 2H), 7.69 (dd, *J* = 5.8, 3.8 Hz, 1H), 7.30 (dd, *J* = 8.0, 4.8 Hz, 1H), 7.25 – 7.14 (m, 2H), 7.07 (s, 1H), 7.02 (s, 1H), 6.22 (d, *J* = 8.0 Hz, 1H), 6.14 (s, 1H), 4.06 – 3.86 (m, 1H), 2.35 (s, 3H), 2.32 (s, 3H), 2.13 – 1.94 (m, 3H), 1.88 – 1.68 (m, 2H), 1.55 – 1.40 (m, 2H), 1.37 – 1.16 (m, 3H). ^{13}C NMR (126 MHz, $CDCl_3$) δ 197.36, 168.01, 166.76, 150.59, 149.11, 139.55, 138.91, 136.94, 130.81, 130.27, 130.10, 129.10, 127.29, 123.56, 62.46, 49.25, 32.88, 32.84, 27.84, 25.51, 24.88, 24.81, 21.22. HRMS (ESI/Q-TOF) m/z: $[M + Na]^+$ calculated for $C_{23}H_{27}N_3O_3$ 416.1945; found 416.1952

***N*-(2-(cyclohexylamino)-2-oxo-1-(pyridin-3-yl)ethyl)-*N*-(4-methoxyphenyl)but-2-ynamide (10b).** Compound was purified using general procedure A, grey solid 83 % yield, 302 mg. ^{1}H NMR (500 MHz, $CDCl_3$) δ 8.50 (dd, *J* = 4.8, 1.7 Hz, 1H), 8.45 (d, *J* = 2.3 Hz, 1H), 7.48 (d, *J* = 8.0 Hz, 1H), 7.12 (ddd, *J* = 8.0, 4.9, 0.9 Hz, 1H), 6.98 (s, 2H), 6.79 – 6.70 (m, 2H), 6.10 (s, 1H), 6.00 (d, *J* = 8.0 Hz, 1H), 3.88 – 3.81 (m, 1H), 3.79 (s, 3H), 1.94 – 1.84 (m, 2H), 1.74 (s, 4H), 1.61 (s, 1H), 1.42 – 1.11 (m, 6H). ^{13}C NMR (126 MHz, $CDCl_3$) δ 167.75, 159.81, 155.97, 151.57, 149.93, 138.74, 132.10, 130.52, 123.44, 114.20, 92.59, 61.98, 55.74, 49.28, 33.21, 33.14, 25.85, 25.10, 4.39.

***N*-(2-(cyclohexylamino)-2-oxo-1-(pyridin-3-yl)ethyl)but-2-ynamide (10c).** Compound was purified using general procedure C, white solid 57 % yield, 153 mg. ^{1}H NMR (500 MHz, $CDCl_3$) δ 8.58 (dd, *J* = 2.4, 0.9 Hz, 1H), 8.50 (dd, *J* = 4.8, 1.6 Hz, 1H), 7.77 – 7.72 (m, 1H), 7.62 (d, *J* = 7.5 Hz, 1H), 7.32 – 7.20 (m, 2H), 5.65 (d, *J* = 7.5 Hz, 1H), 3.74 – 3.63 (m, 1H), 1.93 (s, 3H), 1.75 – 1.64 (m, 3H), 1.63 – 1.52 (m, 2H), 1.36 – 1.16 (m, 2H), 1.14 – 0.98 (m, 3H). ^{13}C NMR (126 MHz, $CDCl_3$) δ 167.88, 153.20, 149.46, 148.97, 135.07, 134.31, 124.12, 85.46, 74.64, 54.99, 49.14, 32.84, 32.68, 25.70, 25.02, 24.90, 3.98.

***N*-(3-acetamidophenyl)-*N*-(2-(cyclohexylamino)-2-oxo-1-(pyridin-3-yl)ethyl)but-2-ynamide (10d).** Compound was purified using general procedure A, white solid 82 % yield, 320 mg. ^{1}H NMR (500 MHz, $CDCl_3$) δ 8.42 (s, 2H), 7.96 (s, 1H), 7.83 – 7.76 (m, 1H), 7.49 (dt, *J* = 7.9, 2.1 Hz, 2H), 7.17 – 7.04 (m, 2H), 6.74 (d, *J* = 7.8 Hz, 1H), 6.34 (d, *J* = 8.1 Hz, 1H), 6.03 (s, 1H), 3.78 – 3.68 (m, 1H), 2.13 (s, 3H),

1.92 (d, *J* = 12.2 Hz, 1H), 1.82 (s, 1H), 1.69 (s, 3H), 1.63 – 1.51 (m, 2H), 1.33 – 1.22 (m, 2H), 1.11 (dtd, *J* = 35.2, 11.2, 3.6 Hz, 3H). ^{13}C NMR (126 MHz, $CDCl_3$) δ 168.57, 167.51, 155.06, 151.09, 149.64, 139.27, 138.81, 137.84, 130.10, 129.22, 125.98, 123.24, 121.38, 119.91, 92.30, 77.29, 77.04, 76.79, 73.69, 62.29, 49.04, 32.69, 25.40, 24.76, 24.71, 24.54, 3.99.

***N*-(4-acetamidophenyl)-*N*-(2-(cyclohexylamino)-2-oxo-1-(pyridin-3-yl)ethyl)but-2-ynamide (10e).** Compound was purified using general procedure A, light brown solid 89 % yield, 345 mg. ^{1}H NMR (500 MHz, $CDCl_3$) δ 8.48 – 8.44 (m, 1H), 8.41 (s, 1H), 7.50 (dt, *J* = 7.6, 1.9 Hz, 1H), 7.43 (d, *J* = 8.4 Hz, 2H), 7.14 (dd, *J* = 8.0, 4.8 Hz, 1H), 7.03 (d, *J* = 7.5 Hz, 2H), 6.24 (s, 1H), 6.09 (s, 1H), 3.81 (dp, *J* = 11.0, 4.0, 3.6 Hz, 1H), 2.15 – 2.12 (m, 3H), 2.01 – 1.91 (m, 1H), 1.89 – 1.82 (m, 1H), 1.78 – 1.64 (m, 4H), 1.64 – 1.52 (m, 1H), 1.45 – 1.05 (m, 6H). ^{13}C NMR (126 MHz, $CDCl_3$) δ 168.74, 167.40, 155.36, 151.06, 149.50, 138.70, 138.23, 134.05, 131.10, 130.16, 123.29, 119.30, 92.50, 77.30, 77.05, 76.79, 73.67, 61.88, 49.01, 32.77, 32.71, 25.42, 24.75, 24.70, 24.57, 4.00.

***N*-(2-(cyclohexylamino)-2-oxo-1-(pyridin-3-yl)ethyl)-*N*-(4-fluorophenyl)but-2-ynamide (10f).** Compound was purified using general procedure A, light brown solid 88 % yield, 311 mg. ^{1}H NMR (500 MHz, $CDCl_3$) δ 8.49 (dd, *J* = 4.8, 1.6 Hz, 1H), 8.44 (d, *J* = 2.3 Hz, 1H), 7.46 (dt, *J* = 8.0, 2.0 Hz, 1H), 7.11 (dt, *J* = 10.7, 5.3 Hz, 2H), 6.91 (t, *J* = 8.6 Hz, 2H), 6.10 (s, 1H), 6.02 (s, 1H), 3.82 (dtd, *J* = 10.8, 7.3, 4.0 Hz, 1H), 2.04 – 1.93 (m, 1H), 1.89 – 1.82 (m, 1H), 1.72 (s, 3H), 1.67 – 1.56 (m, 2H), 1.45 – 1.29 (m, 2H), 1.27 – 1.04 (m, 3H). ^{13}C NMR (126 MHz, $CDCl_3$) δ 167.24, 163.25, 161.27, 155.15, 151.13, 149.73, 138.05, 134.72, 134.69, 132.76, 132.69, 130.05, 123.21, 115.69, 115.51, 92.45, 73.58, 61.42, 49.01, 32.78, 32.72, 25.43, 24.77, 24.71, 3.89.

***N*-(2-(cyclohexylamino)-2-oxo-1-(pyridin-3-yl)ethyl)-*N*-(4-(difluoromethoxy)phenyl)but-2-ynamide (10g).** Compound was purified using general procedure A, light brown solid 89 % yield, 355 mg. ^{1}H NMR (500 MHz, $CDCl_3$) δ 8.51 (dd, *J* = 4.8, 1.6 Hz, 1H), 8.46 (d, *J* = 2.3 Hz, 1H), 7.50 (dt, *J* = 8.0, 2.0 Hz, 1H), 7.20 – 7.10 (m, 2H), 7.03 – 6.93 (m, 2H), 6.50 (t, *J* = 73.4 Hz, 1H), 6.10 (s, 1H), 5.93 (d, *J* = 8.1 Hz, 1H), 3.83 (dtd, *J* = 10.8, 7.7, 7.3, 4.0 Hz, 1H), 1.98 (s, 1H), 1.87 (dd, *J* = 12.1, 4.0 Hz, 1H), 1.76 – 1.71 (m, 4H), 1.70 – 1.57 (m, 2H), 1.45 – 1.28 (m, 2H), 1.24 – 1.03 (m, 3H). ^{13}C NMR (126 MHz, $CDCl_3$) δ 167.53, 155.46, 151.37, 150.03, 138.52, 132.78, 130.44, 123.65, 119.71, 115.88, 92.99, 73.95, 61.89, 49.41, 33.17, 33.11, 25.81, 25.14, 25.09, 4.30, 4.16. ^{19}F NMR (471 MHz, $CDCl_3$) δ -81.48 (d, *J* = 73.5 Hz).

***In vitro* assays.**

Protein production. The DNA sequence encoding 3CL SARS-CoV-2 protease (GI: 1831502838) was synthetized (optimized for expression in *Escherichia coli*) and cloned into a pGEX-6-1 vector between BamHI and XhoI restriction sites, by GenScript (Piscataway, NJ, USA), based on Zhang *et al.* methodology,[44] The protein sequence was preceded by an N-terminal GST sequence and the HRV3C PreScission protease site (SAVLQ↓SGFRK). Autocleavage activity of the enzyme leaves its *N*-terminus starting with the serine after the QS cleavage site (Q↓S). At the C-terminus, based on Xue *et al.*,[45] and Zhang *et al.*[44], the protein was designed to end at the last glutamine comprising the natural C-terminus of the enzyme, followed by a glycine, a proline residue and six histidine residues. The protein this has a 6-His purification tag that can be cleaved using a modified-PreScission protease approach (SGVTFQ↓GP).

E. coli BL21 (DE3) cells were transformed using the plasmid described above and the $CaCl_2$ method[46] and colonies were selected on LB-agar-ampicillin plates. A single colony was picked and grew over night in LB media and then used to inoculate a 400 mL LB culture. This was grown at 37 ºC, 250 rpm, until an optical density at 600 nm of 0.7 (O.D.600) was reached and then induced for 18h at 16 ºC (250 rpm) by adding 0.25 mM IPTG. The bacterial pellet was collected after 4,000 rpm centrifugation and resuspended in 30 mL of 50 mM Tris-HCl pH 8.0, 150 mM NaCl (resuspension buffer). An Ultrasonic Cell Disruption Sonifier 450 (Branson) was used to sonicate the cells (on ice) with 6 pulses of 2 minutes (Output Control 7 and 50 % Duty Cycle).

Buffer A (50 mM Tris-HCl pH 8.0, 150 mM NaCl, 20 mM imidazole) and Buffer B (50 mM Tris-HCl, 150 mM NaCl, 500 mM imidazole) were used for purifying 3CL^{pro} after the clarified supernatant (14,000 rpm centrifugation) was loaded into a 1 mL HisTrap FF (GE Healthcare, IL, USA). 5 mL fractions were collected by washing with single column volumes of increasing imidazole concentration (0, 5, 10, 15, 20, 25, 30, 35, 40, 45 and 50 % Buffer B).

After running SDS-PAGE for confirmation (Mini-PROTEAN® TGX™ Precast Gels, Bio-Rad), two sets of fractions were pooled independently. One of them contained 3CL^{pro} with a high molecular weight contaminant (5 and 10 % Buffer B) while the other contained only the pure enzyme (15, 20 and 25 % buffer B). Imidazole was eliminated from pooled fractions by multiple washes with resuspension buffer using 10K cut-off Amicon® Ultra-15 Centrifugal Filter Units (Millipore Sigma, Burlington, MA, USA). Absorbance at 280 nm was recorded for the pure sample and the protein concentration was estimated to be 8.5 µM (around 0.3 g/L). Based on SDS-PAGE results, the same concentration was assumed for the

other sample. These samples were aliquoted and stored at -20 Celsius degrees. In all the experiments (unless specified) the pure preparation was used. See Figure S1 for more information.

Bulk amount of 3CL^{pro} for crystallization was purified from cell pellets resuspended in a buffer (50mM Tris, 150mM NaCl, 20mM imidazole, pH 8.0). Cell lysate was subsequently centrifuged at 15,000g at 4°C for 20 min. The supernatant was further loaded on a HisTrap HP column (Cytiva) and then purified using a second buffer (50mM Tris, 150mM NaCl, 500 mM imidazole, pH 8.0) on an AKTA Avant purification system (Cytiva). The fractions were pooled, the his-tag removed with Pierce HRV 3C protease (Thermo Scientific) at 4°C for 24 h and dialyzed in buffer A with TCEP at 0.5 mM. The unlabeled protein was loaded again on a HisTrap HP column (Cytiva), the flow-through was collected and dialyzed in a third buffer (20mM Tris, 100mM NaCl, 0.5mM TCEP, pH 8.0). A second step of purification was carried out on a HiTrap Q FF column using the third buffer (20mM Tris, 100mM NaCl, 0.5 mM TCEP, pH 8.0) The fractions were pooled and concentrated to 12 mg/mL.

Detection of inhibitors by fluorescence spectrophotometry. For all inhibition experiments, reactions were performed in 50 µL assay with 11.76 µM fluorescence substrate DABCYL-KTSAVLQSGFRKME-EDANS from BPS Biosciences (San Diego, CA, USA), which has been previously used for assaying 3CL proteases.[47]

38 µL of enzyme (diluted in a 3CL^{pro} Protease Assay Buffer from BPS Bioscience supplemented with 1 mM DTT) were incubated for 30 minutes at room temperature with 2 µL of 1.25 mM compounds (diluted in DMSO; Sigma). In both cases, screenings (duplicates) and IC_{50} experiments (duplicates and triplicates), 10 µL of diluted substrate (58.8 µM) were added and reactions monitored by following the fluorescence as a function of time (excitation at 360 nm, emission at 460 nm) using a Synergy™ H4 Hybrid Multi-Mode Microplate Reader (Winooski, VT, USA). Controls were (i) no inhibition, only DMSO, and (ii) positive inhibition, compound GC376 (BPS Bioscience) diluted in distillate water. In all cases the compounds were added as DMSO solutions and their final concentration in the reactions was 50 µM. The reactions ran for at least one hour, and the linear initial slopes of the progress curves were used to calculate the reaction initial velocity in Relative Fluorescent Units in time (RFU per minute). GraphPad software was used to determine IC_{50} values.

Liquid chromatography-mass spectrometry (LC-MS). Stored-frozen protein samples were buffer exchanged with 5 mM Tris-HCl pH 8.0, 15 mM NaCl buffer using 4K cut-off Amicon® small Centrifugal Filter Units (Millipore Sigma, Burlington, MA, USA) and prepared at 0.1-0.2 mg/mL. 96 µL of this

solution was mixed with 4 µL of 2.5 mM **4a** or **18**. Pure DMSO was used as a negative control. Protein samples were analyzed by LC-MS using a Dionex Ultimate 3000 UHPLC coupled to a Bruker Maxis Impact Q-TOF in positive ESI mode. Samples were separated on an Agilent PLRP-S column (1000Å, 5 µM, 2.1 x 50 mm) heated to 80 ºC at a flow rate of 0.5 ml/min using a gradient of 80% mobile phase A (0.1% formic acid in H2O) and 20% mobile phase B (0.1% formic acid in ACN) for 2 minutes, ramped to 60% mobile phase A and 40% mobile phase B in 5 minutes, and 10% mobile phase A and 90% mobile phase B in 5 minutes. The data was processed and spectra deconvoluted using the Bruker DataAnalysis software version 4.2.

Isothermal Titration Calorimetry (ITC). All ITC experiments were performed on an ITC200 instrument (Malvern Panalytical Ltd, UK) in high-feedback mode with a 1s signal averaging window, a stirring rate of 750 rpm, pre-injection delay of 120 s, and a reference power of 7. A small first injection of 0.2 µL was followed by a 2 µL injections with a wait period of 1400 seconds. The sample cell contained 0.5 mg/mL of the peptide Cbz-TSAVLQSGFRK (CanPeptide, Montreal, QC, Canada) with either 4 µM **4a**, 6.4µM **6k**, 6.4 µM **6i**, or no inhibitor, while the injection syringe contained 54.6 µM 3CL^{pro}. All syringe and sample cell components were dissolved in a 50 mM Tris-HCl pH 8.0, 150 mM NaCl buffer containing 4% DMSO.

Protein crystallization and structure solution. The enzyme was buffer exchanged into 20 mM Tris pH8, 100mM NaCl, 1mM DTT and concentrated to 5mg/ml, and was then incubated with 450 µM of compound **6k** for 1 hour at room temperature. Following incubation, the sample was filtered using a 0.22 µm filter and used for crystallization trials. Crystals were grown using the sitting drop method at 22 °C. 200 nL enzyme was mixed with 200 nL well solution (30% PEG2000 MME, 0.2M Potassium thiocyanate) and allowed to equilibrate against 50 µL well solution. The crystals were cryo-protected using well solution supplemented with 20% ethylene glycol and flash frozen in liquid nitrogen. Data was collected at the Canadian Light Source CMCF-BM beamline and processed in space group C 1 2 1. The structure was solved in PHASER[48] with a previously published structure of the enzyme (6WTK)[49] as a search model. Restraints for the covalently bonded inhibitor were generated using AceDRG[50] in CCP4i2,[51] and the model was refined with REFMAC5[52] and Coot.[53]

Supporting Information

Addition information on LC-MS data, ITC measurement, dose-response curves and ^{1}H and ^{13}C NMR spectra.

Author information

Felipe A. Venegas' current address: Centre for Structural and Functional Genomics and Department of Chemistry and Biochemistry, Concordia University, 7141 Sherbrooke Street West, Montreal, QC, H4B 1R6, Canada

Acknowledgment

We thank the Canadian Institutes of Health Research (CIHR, OV3-170644), the McGill Interdisciplinary Initiative in Infection and Immunity (MI4) and the Faculty of Science for funding.

References

(1) https://www.who.int/.

(2) https://www.ecdc.europa.eu/en/publications-data/distribution-confirmed-cases-mers-cov-place-infection-and-month-onset-march-2012.

(3) Schlottau, K.; Rissmann, M.; Graaf, A.; Schön, J.; Sehl, J.; Wylezich, C.; Höper, D.; Mettenleiter, T. C.; Balkema-Buschmann, A.; Harder, T.; Grund, C.; Hoffmann, D.; Breithaupt, A.; Beer, M. SARS-CoV-2 in fruit bats, ferrets, pigs, and chickens: an experimental transmission study. *Lancet Micr.* **2020**, *1*, E218-E225.

(4) Shi, Z.; Hu, Z. A review of studies on animal reservoirs of the SARS coronavirus. *Virus Res.* **2008**, *133*, 74-87.

(5) https://www.imperial.ac.uk/mrc-global-infectious-disease-analysis/news--wuhan-coronavirus/.

(6) WHO Coronavirus Disease (COVID-19) Dashboard. https://covid19.who.int/ (accessed Oct, 7 2020).

(7) Dai, L.; Gao, G. F. Viral targets for vaccines against COVID-19. *Nat. Rev. Immunol.* **2021**, *21*, 73-82.

(8) Cannalire, R.; Cerchia, C.; Beccari, A. R.; Di Leva, F. S.; Summa, V. Targeting SARS-CoV-2 Proteases and Polymerase for COVID-19 Treatment: State of the Art and Future Opportunities. *J. Med. Chem.* **2020**.

(9) Zhou, P.; Yang, X.-L.; Wang, X.-G.; Hu, B.; Zhang, L.; Zhang, W.; Si, H.-R.; Zhu, Y.; Li, B.; Huang, C.-L.; Chen, H.-D.; Chen, J.; Luo, Y.; Guo, H.; Jiang, R.-D.; Liu, M.-Q.; Chen, Y.; Shen, X.-R.; Wang, X.; Zheng, X.-S.; Zhao, K.; Chen, Q.-J.; Deng, F.; Liu, L.-L.; Yan, B.; Zhan, F.-X.; Wang, Y.-Y.; Xiao, G.-F.; Shi, Z.-L. A pneumonia outbreak associated with a new coronavirus of probable bat origin. *Nature* **2020**, *579*, 270-273.

(10) Wu, A.; Peng, Y.; Huang, B.; Ding, X.; Wang, X.; Niu, P.; Meng, J.; Zhu, Z.; Zhang, Z.; Wang, J.; Sheng, J.; Quan, L.; Xia, Z.; Tan, W.; Cheng, G.; Jiang, T. Genome Composition and Divergence of the Novel Coronavirus (2019-nCoV) Originating in China. *Cell Host & Microbe* **2020**.

(11) Rathnayake, A. D.; Kim, Y.; Dampalla, C. S.; Nguyen, H. N.; Jesri, A.-R. M.; Kashipathy, M. M.; Lushington, G. H.; Battaile, K. P.; Lovell, S.; Chang, K.-O.; Groutas, W. C. Structure-Guided Optimization of Dipeptidyl Inhibitors of Norovirus 3CL Protease. *J. Med. Chem.* **2020**.

(12) Kuo, C.-J.; Shie, J.-J.; Fang, J.-M.; Yen, G.-R.; Hsu, J. T. A.; Liu, H.-G.; Tseng, S.-N.; Chang, S.-C.; Lee, C.-Y.; Shih, S.-R.; Liang, P.-H. Design, synthesis, and evaluation of 3C protease inhibitors as anti-enterovirus 71 agents. *Bioorg. Med. Chem.* **2008**, *16*, 7388-7398.

(13) Dragovich, P. S.; Prins, T. J.; Zhou, R.; Webber, S. E.; Marakovits, J. T.; Fuhrman, S. A.; Patick, A. K.; Matthews, D. A.; Lee, C. A.; Ford, C. E.; Burke, B. J.; Rejto, P. A.; Hendrickson, T. F.; Tuntland, T.; Brown, E. L.; Meador, J. W.; Ferre, R. A.; Harr, J. E. V.; Kosa, M. B.; Worland, S. T. Structure-Based Design, Synthesis,

and Biological Evaluation of Irreversible Human Rhinovirus 3C Protease Inhibitors. 4. Incorporation of P1 Lactam Moieties as l-Glutamine Replacements. *J. Med. Chem.* **1999**, *42*, 1213-1224.

(14) Pillaiyar, T.; Manickam, M.; Namasivayam, V.; Hayashi, Y.; Jung, S.-H. An Overview of Severe Acute Respiratory Syndrome–Coronavirus (SARS-CoV) 3CL Protease Inhibitors: Peptidomimetics and Small Molecule Chemotherapy. *J. Med. Chem.* **2016**, *59*, 6595-6628.

(15) Zaidman, D.; Gehrtz, P.; Filep, M.; Fearon, D.; Prilusky, J.; Duberstein, S.; Cohen, G.; Owen, D.; Resnick, E.; Strain-Damerell, C.; Lukacik, P.; Barr, H.; Walsh, M. A.; von Delft, F.; London, N. An automatic pipeline for the design of irreversible derivatives identifies a potent SARS-CoV-2 Mpro inhibitor. *bioRxiv* **2020**, 2020.2009.2021.299776.

(16) Anand, K.; Ziebuhr, J.; Wadhwani, P.; Mesters, J. R.; Hilgenfeld, R. Coronavirus Main Proteinase (3CLpro) Structure: Basis for Design of Anti-SARS Drugs. *Science* **2003**, *300*, 1763-1767.

(17) Liu, C.; Zhou, Q.; Li, Y.; Garner, L. V.; Watkins, S. P.; Carter, L. J.; Smoot, J.; Gregg, A. C.; Daniels, A. D.; Jervey, S.; Albaiu, D. Research and Development on Therapeutic Agents and Vaccines for COVID-19 and Related Human Coronavirus Diseases. *ACS Cent. Sci.* **2020**, *6*, 315-331.

(18) Westberg, M.; Su, Y.; Zou, X.; Ning, L.; Hurst, B.; Tarbet, B.; Lin, M. Z. Rational design of a new class of protease inhibitors for the potential treatment of coronavirus diseases. *bioRxiv* **2020**, 2020.2009.2015.275891.

(19) Iketani, S.; Forouhar, F.; Liu, H.; Hong, S. J.; Lin, F.-Y.; Nair, M. S.; Zask, A.; Huang, Y.; Xing, L.; Stockwell, B. R.; Chavez, A.; Ho, D. D. Lead compounds for the development of SARS-CoV-2 3CL protease inhibitors. *bioRxiv* **2020**, 2020.2008.2003.235291.

(20) Boras, B.; Jones, R. M.; Anson, B. J.; Arenson, D.; Aschenbrenner, L.; Bakowski, M. A.; Beutler, N.; Binder, J.; Chen, E.; Eng, H.; Hammond, J.; Hoffman, R.; Kadar, E. P.; Kania, R.; Kimoto, E.; Kirkpatrick, M. G.; Lanyon, L.; Lendy, E. K.; Lillis, J. R.; Luthra, S. A.; Ma, C.; Noell, S.; Obach, R. S.; O' Brien, M. N.; O'Connor, R.; Ogilvie, K.; Owen, D.; Pettersson, M.; Reese, M. R.; Rogers, T. F.; Rossulek, M. I.; Sathish, J. G.; Steppan, C.; Ticehurst, M.; Updyke, L. W.; Zhu, Y.; Wang, J.; Chatterjee, A. K.; Mesecar, A. D.; Anderson, A. S.; Allerton, C. Discovery of a Novel Inhibitor of Coronavirus 3CL Protease as a Clinical Candidate for the Potential Treatment of COVID-19. *bioRxiv* **2020**, 2020.2009.2012.293498.

(21) Hoffman, R.; Kania, R. S.; Brothers, M. A.; Davies, J. F.; Ferre, R. A.; Gajiwala, K. S.; He, M.; Hogan, R. J.; Kozminski, K.; Li, L. Y.; Lockner, J. W.; Lou, J.; Marra, M. T.; Mitchell, L. J. J.; Murraya, B. W.; Nieman, J. A.; Noell, S.; Planken, S. P.; Rowe, T.; Ryan, K.; Smith, G. J. I.; Solowiej, J. E.; Steppan, C. M.; Taggart, B. The Discovery of Ketone-Based Covalent Inhibitors of Coronavirus 3CL Proteases for the Potential Therapeutic Treatment of COVID-19. *ChemRxiv* **2020**, *https://doi.org/10.26434/chemrxiv.12631496.v1*

(22) Hoffman, R. L.; Kania, R. S.; Brothers, M. A.; Davies, J. F.; Ferre, R. A.; Gajiwala, K. S.; He, M.; Hogan, R. J.; Kozminski, K.; Li, L. Y.; Lockner, J. W.; Lou, J.; Marra, M. T.; Mitchell, L. J.; Murray, B. W.; Nieman, J. A.; Noell, S.; Planken, S. P.; Rowe, T.; Ryan, K.; Smith, G. J.; Solowiej, J. E.; Steppan, C. M.; Taggart, B. Discovery of Ketone-Based Covalent Inhibitors of Coronavirus 3CL Proteases for the Potential Therapeutic Treatment of COVID-19. *J. Med. Chem.* **2020**, *63*, 12725-12747.

(23) Chen, L.-R.; Wang, Y.-C.; Lin, Y. W.; Chou, S.-Y.; Chen, S.-F.; Liu, L. T.; Wu, Y.-T.; Kuo, C.-J.; Chen, T. S.-S.; Juang, S.-H. Synthesis and evaluation of isatin derivatives as effective SARS coronavirus 3CL protease inhibitors. *Bioorg. Med. Chem. Lett.* **2005**, *15*, 3058-3062.

(24) Zhang, J.; Huitema, C.; Niu, C.; Yin, J.; James, M. N. G.; Eltis, L. D.; Vederas, J. C. Aryl methylene ketones and fluorinated methylene ketones as reversible inhibitors for severe acute respiratory syndrome (SARS) 3C-like proteinase. *Bioorg. Chem.* **2008**, *36*, 229-240.

(25) Zhang, C.-H.; Stone, E. A.; Deshmukh, M.; Ippolito, J. A.; Ghahremanpour, M. M.; Tirado-Rives, J.; Spasov, K. A.; Zhang, S.; Takeo, Y.; Kudalkar, S. N.; Liang, Z.; Isaacs, F.; Lindenbach, B.; Miller, S. J.; Anderson, K. S.; Jorgensen, W. L. Potent Noncovalent Inhibitors of the Main Protease of SARS-CoV-2 from Molecular Sculpting of the Drug Perampanel Guided by Free Energy Perturbation Calculations. *ACS Cent. Sci.* **2021**.

(26) Halford, B. Pfizer's novel COVID-19 antiviral heads to clinical trials. *C&EN* **2020**, *Sept 17*.

(27) Drayman, N.; Jones, K. A.; Azizi, S.-A.; Froggatt, H. M.; Tan, K.; Maltseva, N. I.; Chen, S.; Nicolaescu, V.; Dvorkin, S.; Furlong, K.; Kathayat, R. S.; Firpo, M. R.; Mastrodomenico, V.; Bruce, E. A.; Schmidt,

M. M.; Jedrzejczak, R.; Muñoz-Alía, M. Á.; Schuster, B.; Nair, V.; Botten, J. W.; Brooke, C. B.; Baker, S. C.; Mounce, B. C.; Heaton, N. S.; Dickinson, B. C.; Jaochimiak, A.; Randall, G.; Tay, S. Drug repurposing screen identifies masitinib as a 3CLpro inhibitor that blocks replication of SARS-CoV-2 in vitro. *bioRxiv* **2020**, 2020.2008.2031.274639.

(28) Zhu, W.; Xu, M.; Chen, C. Z.; Guo, H.; Shen, M.; Hu, X.; Shinn, P.; Klumpp-Thomas, C.; Michael, S. G.; Zheng, W. Identification of SARS-CoV-2 3CL Protease Inhibitors by a Quantitative High-Throughput Screening. *ACS Pharmacol. Transl. Sci.* **2020**.

(29) De Cesco, S.; Kurian, J.; Dufresne, C.; Mittermaier, A.; Moitessier, N. Covalent inhibitors design and discovery. *Eur. J. Med. Chem.* **2017**, *138*, 96-114.

(30) Zhou, S.; Chan, E.; Duan, W.; Huang, M.; Chen, Y. Z. Drug bioactivation, covalent binding to target proteins and toxicity relevance. *Drug Metab. Rev.* **2005**, 41-213.

(31) Guterman, L. Covalent Drugs Form Long-Lived Ties. *C&EN* **2011**, *89*, 19-26.

(32) Tang, B.; He, F.; Liu, D.; Fang, M.; Wu, Z.; Xu, D. AI-aided design of novel targeted covalent inhibitors against SARS-CoV-2. *bioRxiv* **2020**, 2020.2003.2003.972133.

(33) Nguyen, D. D.; Gao, K.; Chen, J.; Wang, R.; Wei, G.-W. Potentially highly potent drugs for 2019-nCoV. *bioRxiv* **2020**, 2020.2002.2005.936013.

(34) Roy, R.; Sk, M. F.; Jonniya, N. A.; Poddar, S.; Kar, P. Finding Potent Inhibitors Against SARS-CoV-2 Main Protease Through Virtual Screening, ADMET, and Molecular Dynamic Simulation Studies. . *ChemRxiv* **2020**, *Preprint*.

(35) Mariaule, G.; De Cesco, S.; Airaghi, F.; Kurian, J.; Schiavini, P.; Rocheleau, S.; Huskić, I.; Auclair, K.; Mittermaier, A.; Moitessier, N. 3-Oxo-hexahydro-1H-isoindole-4-carboxylic acid as a drug chiral bicyclic scaffold: structure-based design and preparation of conformationally constrained covalent and noncovalent prolyl oligopeptidase inhibitors. *J. Med. Chem.* **2016**, *59*, 4221–4234.

(36) Plescia, J.; Dufresne, C.; Janmamode, N.; Wahba, A. S.; Mittermaier, A. K.; Moitessier, N. Discovery of covalent prolyl oligopeptidase boronic ester inhibitors. *Eur. J. Med. Chem.* **2020**, *185*, 111783.

(37) Jacobs, J.; Grum-Tokars, V.; Zhou, Y.; Turlington, M.; Saldanha, S. A.; Chase, P.; Eggler, A.; Dawson, E. S.; Baez-Santos, Y. M.; Tomar, S.; Mielech, A. M.; Baker, S. C.; Lindsley, C. W.; Hodder, P.; Mesecar, A.; Stauffer, S. R. Discovery, Synthesis, And Structure-Based Optimization of a Series of N-(tert-Butyl)-2-(N-arylamido)-2-(pyridin-3-yl) Acetamides (ML188) as Potent Noncovalent Small Molecule Inhibitors of the Severe Acute Respiratory Syndrome Coronavirus (SARS-CoV) 3CL Protease. *J. Med. Chem.* **2013**, *56*, 534-546.

(38) Moitessier, N.; Pottel, J.; Therrien, E.; Englebienne, P.; Liu, Z.; Tomberg, A.; Corbeil, C. R. Medicinal chemistry projects requiring imaginative structure-based drug design methods. *Acc. Chem. Res.* **2016**, *49*, 1646-1657.

(39) Behnke, D.; Taube, R.; Illgen, K.; Nerdinger, S.; Herdtweck, E. Substituted 2-(Cyanomethyl-amino)-acetamides by a Novel Three-Component Reaction. *Synlett* **2004**, *2004*, 688-692.

(40) Gedey, S.; Van der Eycken, J.; Fülöp, F. Liquid-Phase Combinatorial Synthesis of Alicyclic β-Lactams via Ugi Four-Component Reaction. *Org. Lett.* **2002**, *4*, 1967-1969.

(41) St John, S. E.; Mesecar, A. D. Broad spectrum non-covalent coronavirus protease inhibitors. USA Patent.

(42) Turlington, M.; Chun, A.; Tomar, S.; Eggler, A.; Grum-Tokars, V.; Jacobs, J.; Daniels, J. S.; Dawson, E.; Saldanha, A.; Chase, P.; Baez-Santos, Y. M.; Lindsley, C. W.; Hodder, P.; Mesecar, A. D.; Stauffer, S. R. Discovery of N-(benzo[1,2,3]triazol-1-yl)-N-(benzyl)acetamido)phenyl) carboxamides as severe acute respiratory syndrome coronavirus (SARS-CoV) 3CLpro inhibitors: Identification of ML300 and noncovalent nanomolar inhibitors with an induced-fit binding. *Bioorg. Med. Chem. Lett.* **2013**, *23*, 6172-6177.

(43) Di Trani, J. M.; De Cesco, S.; O'Leary, R.; Plescia, J.; do Nascimento, C. J.; Moitessier, N.; Mittermaier, A. K. Rapid measurement of inhibitor binding kinetics by isothermal titration calorimetry. *Nat. Commun.* **2018**, *9*, 893.

(44) Zhang, L.; Lin, D.; Sun, X.; Curth, U.; Drosten, C.; Sauerhering, L.; Becker, S.; Rox, K.; Hilgenfeld, R. Crystal structure of SARS-CoV-2 main protease provides a basis for design of improved α-ketoamide inhibitors. *Science* **2020**, *368*, 409-412.

(45) Xue, X.; Yang, H.; Shen, W.; Zhao, Q.; Li, J.; Yang, K.; Chen, C.; Jin, Y.; Bartlam, M.; Rao, Z. Production of Authentic SARS-CoV Mpro with Enhanced Activity: Application as a Novel Tag-cleavage Endopeptidase for Protein Overproduction. *J. Mol. Biol.* **2007**, *366*, 965-975.

(46) Hanahan, D. Studies on transformation of Escherichia coli with plasmids. *J Mol Biol* **1983**, *166*, 557-580.

(47) Chen, S.; Chen, L.-l.; Luo, H.-b.; Sun, T.; Chen, J.; Ye, F.; Cai, J.-h.; Shen, J.-k.; Shen, X.; Jiang, H.-l. Enzymatic activity characterization of SARS coronavirus 3C-like protease by fluorescence resonance energy transfer technique. *Acta Pharmacologica Sinica* **2005**, *26*, 99-106.

(48) McCoy, A. J.; Grosse-Kunstleve, R. W.; Adams, P. D.; Winn, M. D.; Storoni, L. C.; Read, R. J. Phaser crystallographic software. *J. Appl. Crystallogr.* **2007**, *40*, 658-674.

(49) Vuong, W.; Khan, M. B.; Fischer, C.; Arutyunova, E.; Lamer, T.; Shields, J.; Saffran, H. A.; McKay, R. T.; van Belkum, M. J.; Joyce, M. A.; Young, H. S.; Tyrrell, D. L.; Vederas, J. C.; Lemieux, M. J. Feline coronavirus drug inhibits the main protease of SARS-CoV-2 and blocks virus replication. *Nat. Commun.* **2020**, *11*, 4282.

(50) Long, F.; Nicholls, R. A.; Emsley, P.; Graæulis, S.; Merkys, A.; Vaitkus, A.; Murshudov, G. N. Validation and extraction of molecular-geometry information from small-molecule databases. *Acta Crystallogr. D Struct. Biol.* **2017**, *73*, 103-111.

(51) Potterton, L.; Agirre, J.; Ballard, C.; Cowtan, K.; Dodson, E.; Evans, P. R.; Jenkins, H. T.; Keegan, R.; Krissinel, E.; Stevenson, K.; Lebedev, A.; McNicholas, S. J.; Nicholls, R. A.; Noble, M.; Pannu, N. S.; Roth, C.; Sheldrick, G.; Skubak, P.; Turkenburg, J.; Uski, V.; von Delft, F.; Waterman, D.; Wilson, K.; Winn, M.; Wojdyr, M. CCP4i2: the new graphical user interface to the CCP4 program suite. *Acta Crystallogr. D Struct. Biol.* **2018**, *74*, 68-84.

(52) Skubák, P.; Murshudov, G. N.; Pannu, N. S. Direct incorporation of experimental phase information in model refinement. *Acta Crystallogr. D Biol. Crystallogr.* **2004**, *60*, 2196-2201.

(53) Emsley, P.; Cowtan, K. Coot: model-building tools for molecular graphics. *Acta Crystallogr. D Biol. Crystallogr.* **2004**, *60*, 2126-2132.